Identification of low fluoride areas using conceptual groundwater flow model and hydrogeochemical system analysis in the aquifer system on the flanks of an active volcano: Mount Meru, Northern Tanzania

George Bennett, Jill van Reybrouck, Ceven Shemsanga, Mary Kisaka, Ines Tomašek, Karen Fontijn, Matthieu Kervyn, Kristine Walraevens

Identification of low fluoride areas using conceptual groundwater flow model and hydrogeochemical system analysis in the aquifer system on the flanks of an active volcano: Mount Meru, Northern Tanzania

George Bennett[a,b,*], Jill Van Reybrouck[a], Ceven Shemsanga[c], Mary Kisaka[c,d], Ines Tomašek[d,e,f,g], Karen Fontijn[h], Matthieu Kervyn[d], Kristine Walraevens[a]

[a]*Laboratory for Applied Geology and Hydrogeology, Department of Geology, Ghent University, Belgium*

[b]*Department of Mining and Mineral Processing Engineering, University of Dodoma, Tanzania*

[c]*Department of Geology, University of Dodoma, Tanzania*

[d]*Physical Geography (FARD), Department of Geography, Vrije Universiteit Brussel, Belgium*

[e]*Analytical, Environmental and Geochemistry (AMGC), Department of Chemistry, Vrije Universiteit Brussel, Belgium*

[f]*Laboratoire Magmas et Volcans, CNRS, IRD, OPGC, Université Clermont Auvergne, France*

[g]*Institute of Genetic Reproduction and Development, CNRS UMR 6293, INSERM U1103, Université Clermont Auvergne, France*

[h]*Laboratoire G-Time, Department of Geosciences, Environment and Society, Université libre de Bruxelles, Belgium*

* Corresponding author at: Laboratory for Applied Geology and Hydrogeology, Department of Geology, Ghent University, Belgium.

Email addresses: george.bennett@udom.ac.tz, George.Bennett@UGent.be (G. Bennett)

Abstract

This study investigates the localities of low and high F^- groundwaters in the aquifer system on the flanks of Mount Meru to come up with guidelines to provide groundwater that can be used for drinking water supply without health impacts on the population. Our study focuses on parts of the flanks which were only partially or not at all covered by previous research. Results show that the groundwater chemistry of F^--rich $NaHCO_3$ alkaline groundwater in the area is controlled by dissolution of weathering aluminosilicate minerals (especially Na-K-feldspars), dissolution of F^--bearing minerals, the precipitation of carbonate minerals as secondary products and the dissolution of magmatic gases. Evaporative concentration of solutes, precipitation and redissolution of evaporitic salts may locally play a role, especially on the north-eastern flank of Mount Meru. The low F^- groundwaters which can be used for drinking water supply without health impacts under the WHO limit (1.5 mg/L) are the low-fluoride springs from the high-altitude recharge areas on the eastern and north-western flanks of Mount

Meru inside Arusha National Park, whereas on the western flank the groundwater meets the Tanzanian limit (4.0 mg/L). On the south-western flank, the shallow aquifer composed of alluvium deposits at lower elevations, shows F^- values that meet the Tanzanian limit. One of the three investigated deep boreholes on this flank also meets the Tanzanian limit, this suggests a possibility of finding more localities of relatively low F^- groundwaters in the deep aquifer. Yet, in general, the deposits at lower elevations (the debris avalanche deposits, mantling ash, alluvial fan deposits and lake deposits) are found to contain high to very high F^- values, whereas the deposits at high elevations (pyroclastics and lavas) contain groundwater of low F^- values. Thus, the internal texture and grain size of geological formations (causing variable weatherability), the burial depth of these formations (less weathering at depth) and the water residence times are the factors determining the groundwater mineralisation and F^- concentrations in the area. The study identified that the deep hydrothermal system (volcanic emissions) has influence on the high F^- groundwaters on the eastern and north-eastern flanks of Mount Meru.

Keywords: alkaline groundwater; high-fluoride groundwater; hydrogeochemical processes; volcanic aquifer; Mount Meru; Tanzania; East African Rift System.

1. Introduction

In the Arusha volcanic region in northern Tanzania, around Mount Meru, several studies with focus on F^- concentration in surface water (Kilham and Hecky, 1973; Nanyaro et al., 1984; Kitalika et al. 2018) and groundwater (Ghiglieri et al., 2012; Chacha et al., 2018; Makoba and Muzuka, 2019; Bennett et al., 2021) have been conducted. The studies found that the general groundwater chemistry is F^--rich $NaHCO_3$ alkaline water. The main findings of these studies have been briefly summarised in the study of Bennett et al. (2021), which described the hydrochemical characterisation of high-fluoride groundwater on the eastern, northern, western and south-western flanks of Mount Meru, the subject of a parallel to this paper. The studies that focused on the groundwater chemistry in the area found that rock mineral dissolution, water residence times (Ghiglieri et al., 2012; Chacha et al., 2018; Makoba and Muzuka, 2019; Ijumulana et al., 2020), exchange processes, calcite precipitation (Ghiglieri et al., 2012) and climatic conditions (temperature and rainfall), attributed to altitude and geographic positions (windward and leeward sides of Mount Meru) (Makoba and Muzuka, 2019) are controlling the groundwater chemistry in the area.

The study by Ijumulana et al. (2020) found that the largest regional fluoride hotspot in Northern

Tanzania is originating around Mount Meru with very low probability of finding safe drinking water around the area. The study reported that one of the challenges affecting the blending technology adopted by Arusha Urban Water Supply Authority (AUWASA) is the presence of many sources with high and few with low fluoride concentrations. They measured fluoride concentration of 4.6 mg/L at the blending tank as the net mass of fluoride in drinking water supplied throughout the Arusha City on the south flank of Mount Meru. This concentration is above both WHO limit (1.5 mg/L) (WHO, 2017) and Tanzanian limit (4.0 mg/L) (Tanzania Bureau of Standards, 2008). Also, the study by Bennett et al. (2021) found that 59% of the inventoried usable groundwater points are used to provide drinking water to the local community despite their high F^- values, which exceed both WHO and Tanzanian limits, as most local people do not have any alternative for drinking water. Other than high F^- values, the study by Tomašek et al. (2022) found elevated levels of multiple potentially toxic elements (*i.e.*, Molybdenum and Uranium) in some of the analysed sources, pose another health concern to the local communities. Therefore, the present research investigates the localities of low F^- groundwaters using conceptual groundwater flow model and hydrogeochemical analysis approach on the eastern, northern, western and south-western flanks of Mount Meru based on the results of Bennett et al. (2021), in order to identify and locate the groundwater sources that can be used for drinking water supply without health impacts on the population.

2. Materials and Methods

2.1. Study area

2.1.1. Location, topography, and climate

The study area covers most of the slopes of Mount Meru, and occupies about 1000 km^2 (Fig. 1) (Bennett et al., 2021). Mount Meru is in Arusha region, northern Tanzania. It situated partly in the Arusha National Park just north of the city of Arusha, and 70 km west of Mount Kilimanjaro. The study area covers most parts of the Arusha and Meru districts, each with population of 323,198 and 268,144 inhabitants respectively (Tanzania National Bureau of Statistics, 2013, p.26).

The topography of the study area is dominated by Mount Meru. Its eastern flank is incised by a deep valley formed by a catastrophic sector collapse now occupied by an ash cone that last erupted in 1910 (Delcamp et al., 2017). Numerous parasitic cones are prominent features in the vicinity (Wilkinson et al., 1983; Delcamp et al., 2017; Scoon, 2018).

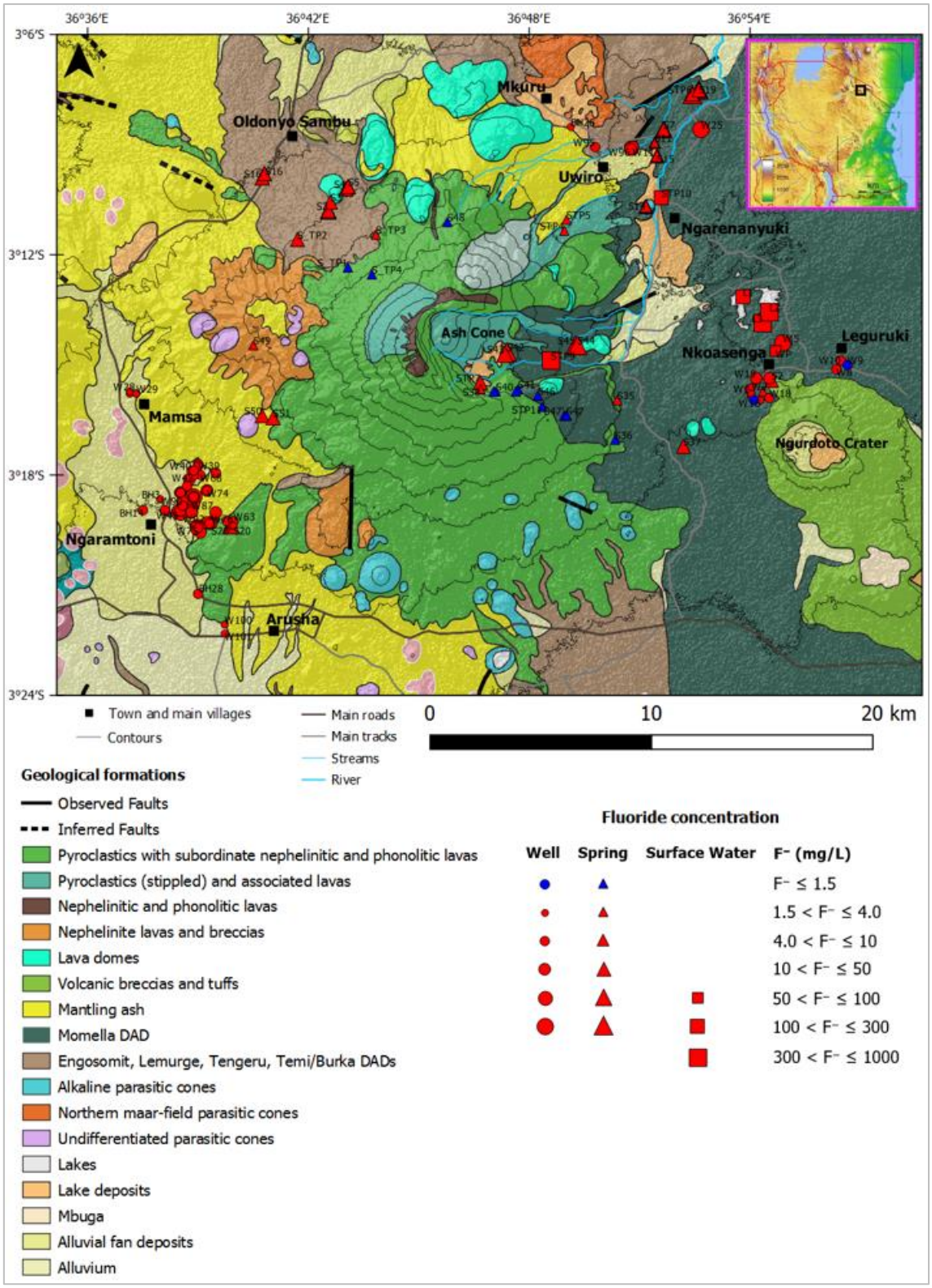

Fig. 1. Geological map of the study area adapted from Bennett et al. (2021), indicating different geological formations and spatial distribution of F^- concentrations of sampled water points. A small map inserted in the top right corner is the map of Tanzania (modified after Mapsland (2021), the original image is under Creative Commons Attribution-ShareAlike 3.0 Unported (CC BY-SA 3.0) license), showing the location of Mount Meru using a black lined square box.

105 The study area experiences a bimodal rainfall pattern; the long "masika" rains extend from late
106 February to late May and the short "vuli" rains from early November to early January. The dry
107 "kiangazi" season is from June to October (Bennett et al., 2021). The average annual rainfall
108 on the southern flank, south-western flank, western flank and north-eastern flank in mm are:
109 962, 958, 905 and 638 respectively (Bennett et al., 2021). The eastern and southern flanks
110 (windward sides) experience a subtropical highland climate, whereas the northern flank
111 (leeward side) experiences a semi-arid climate (steppe climate). The temperature normally
112 ranges from 13 – 30°C with an average annual value of about 25°C (Chacha et al., 2018).

113 ***2.1.2. Geological and hydrogeological setting***

114 The geology of the study area, and the link between the local geology and hydrogeology in the
115 area has been described in Bennett et al. (2021). Mount Meru is an active stratovolcano located
116 within the Northern Tanzanian Divergence Zone of the eastern branch of the East African Rift.
117 The lithology in the study area is dominated by volcanic rocks – lava flows, pyroclastic and
118 debris avalanche deposits from the Mount Meru, with some alluvium, alluvial fan and lake
119 deposits found around the volcano base (Fig. 1). The study by Bennett et al. (2021) described
120 both shallow and deep aquifers on the north-eastern and south-western flanks, but limited only
121 to shallow aquifer on the far east of the eastern flank (*i.e.*, on the northern flank of Ngurdoto
122 crater) and on the western flank. The shallow aquifer on the north-eastern flank is mainly
123 composed of debris avalanche deposits, whereas on the south-western flank is composed by
124 pyroclastic deposits. The deep aquifer on the north-eastern flank is composed of weathered
125 fractured lava, whereas on the south-western flank, it is composed of weathered fractured lava
126 and weathered pyroclastic deposits. The shallow unconfined aquifers on the western flank and
127 far east of the eastern flank are composed of weathered fractured lava and debris avalanche
128 deposits, respectively (Bennett et al., 2021). The groundwater flow paths in the study area are
129 controlled by the geomorphology of the landscape. On each flank, the general groundwater
130 flow system is involving a multidirectional flow from the higher elevation areas towards the
131 lower areas (Bennett et al., 2021).

132 ***2.2. Inventory of water points, sampling, and laboratory analysis***

133 The inventory of water points has been discussed in details in Bennett et al. (2021). The water
134 points are distributed in six clusters: south-western flank (at Ngaramtoni and near Arusha
135 town), western flank (at Mamsa), north-western flank (at Oldonyo Sambu), north-eastern flank
136 (Mkuru, Uwiro and Ngarenanyuki), eastern flank (inside Arusha National Park) and far east of
137 the eastern flank (Nkoasenga and Leguruki). A total of 181 water samples were collected and

analysed, they consist of 175 groundwater and 6 surface water samples. Laboratory analyses have been performed at the Laboratory for Applied Geology and Hydrogeology at Ghent University according to standard methods (APHA et al., 2017). Details are described in Bennett et al. (2021).

2.3. Data processing and analysis

The hydrogeochemical processes and mechanisms controlling the chemical characteristics of groundwater in the study area have been investigated based on the analysis of bivariate diagrams, statistical analyses and hydrogeochemical reactions.

To distinguish whether F^- in the groundwater is derived from chemical weathering of rocks or derived from the atmosphere (due to air pollution), the F^-/Cl^- ratio (by meq/l) proposed by Kilham and Hecky (1973) was used. If the ratio exceeds 0.10, then the F^- originates solely from chemical weathering of rocks.

The activity of dissolved ions and the saturation index (SI) for various mineral phases were computed to analyse the equilibrium status of groundwater, using the geochemical modelling software PHREEQC Interactive for Windows, Version 3.5.0.14000 (Parkhurst and Appelo, 2013).

3. Results and Discussion

3.1. Groundwater hydrochemical composition along the flow path

Hydrochemical analysis shows that the main groundwater type in the study area is F^--rich $NaHCO_3$ alkaline groundwater (average pH = 7.8) (Bennett et al., 2021). Table 1 shows the average values of pH, major and minor ions, and TDS in the water samples from different elevations on different flanks of Mount Meru. The raw analytical data are given in Table 9 in the Appendix. Overall, the groundwater mineralisation increases with residence times along the flow path, this has been discussed in detail by Bennett et al. (2021). These results together with hydrogeochemical processes, spring settings and groundwater level in the wells, were used to develop simplified groundwater flow conceptual models (Tóth, 1963; Tóth, 1999) for the north-eastern flank (Fig. 2), far east of the eastern flank (*i.e.*, on the northern flank of Ngurdoto crater) (Fig. 3), north-western flank (Fig. 4) and south-western flank (Fig. 5). There is not enough data to develop a good representative groundwater flow conceptual model for the western flank, as there is only one spring in the upstream and three shallow wells in the downstream. The shallow wells are close to each other.

Table 1. Average values of pH, major and minor ions, and TDS in the water samples from different elevations on different flanks of Mount Meru (* as mg/L HCO_3^-).

Region	Water source	Number of samples	Average Elevation (m)	Average Well depth (m)	Average pH	Average concentrations (mg/L)										Average TDS (mg/L)
						Na^+	K^+	Ca^{2+}	Mg^{2+}	$(HCO_3^-+CO_3^{2-})$*	SO_4^{2-}	Cl^-	F^-	NO_3^-	NO_2^-	
Eastern flank	Springs	8	2566		7.6	32.9	14.6	7.5	0.5	113	0.95	5.1	3.9	2.1	0.000	220
	Hydrothermal springs	2	2527		8.4	1011	198	6.1	2.0	1728	339	124	198	1.7	0.002	3642
	Springs	3	2183		7.3	21.2	11.9	2.1	0.3	74.7	0.01	4.7	0.4	3.8	0.002	158
	Stream	1	2132		9.1	1140	220	9.1	2.2	914	377	295	553	1.1	0.000	3540
	Springs	2	1953		8.4	413	54.7	1.5	0.4	323	67.9	17.8	264	2.1	0.006	1174
		3	1595		7.8	42.6	17.4	7.8	0.4	135.9	1.42	5.1	5.8	1.5	0.000	264
	Lakes	3	1430		9.8	3786	599	6.8	2.7	7811	209	379	736	6.0	0.032	13541
North-eastern flank	Springs	2	1705		6.9	60.9	8.2	1.6	0.4	154	7.3	3.1	4.2	4.6	0.160	286
		13	1430		7.6	185	39.2	17.6	5.4	524	39.5	14.2	8.0	10.1	0.431	916
		4	1402		8.1	451	57.1	12.0	2.6	905	139	27.8	56.3	43.0	0.046	1819
		8	1332		8.2	785	104	11.4	3.6	1425	435	113	58.9	14.6	0.181	2984
	Shallow wells	1	1551	48	7.7	80.4	12.4	6.3	1.0	220	1.9	3.8	3.6	36.5	0.010	412
		10	1452	8	8.0	210	25.8	6.1	1.2	479	30.8	25.0	17.1	4.9	0.071	891
		1	1399	27	8.5	579	80.9	8.3	6.4	1080	204	78.3	121	12.7	0.000	2322
	River	1	1443		8.8	464	87.2	9.3	1.2	645	126	45.1	144	1.1	0.002	1544
Far east of the eastern flank (Northern flank of Ngurdoto crater)	Springs	1	1560		7.2	106	26.2	14.0	2.4	334	19.8	13.4	2.6	10.0	0.002	573
		1	1483		7.6	171	42.8	2.4	0.4	478	25.7	3.3	10.7	23.5	0.078	789
	Shallow wells	7	1586	8	7.7	94	27.5	12.4	2.4	295	22.6	9.5	3.5	11.6	0.347	605
		3	1491	12	8.2	251	50.8	4.5	1.2	508	35.6	10.9	68.6	44.3	0.000	1118
		3	1354	8	7.7	111	33.5	16.2	3.7	346	29.9	11.8	4.6	26.0	0.002	666
	Water pond	1	1429		9.2	789	269	25.7	5.65	1730	254	62.1	85.9	5.9	0.1264	3237
North-western flank	Springs	4	2567		7.9	32.2	11	3.3	0.6	111	0.3	4.7	0.8	0.9	0.001	242
		15	2084		7.6	91.5	19.6	2.9	0.6	185	8.8	4.1	24.4	8.4	0.328	410
		6	1838		7.1	99.1	24.6	3.2	0.5	235	8.7	4.1	24.8	5.2	0.022	446
Western flank	Spring	1	2240		8.4	111	23.4	16.4	3.1	365	14	7.7	3.4	6.0	0.004	590
	Shallow wells	6	1649	44	7.8	180	39.9	39.7	6.1	539	75.1	25.7	3.7	36.7	2.743	1017
South-western flank	Springs	2	1921		7.9	76.4	22.8	4.4	0.7	212	7.5	6.1	12	3.0	0.020	386
		10	1566		7.8	182	60	21.7	4.9	539	23.4	16.6	8.1	37.0	0.160	1012
	Shallow wells	3	1631	16	7.3	160	30.8	10.2	1.4	439	24.5	9	6.3	20.8	0.150	744
		51	1548	19	7.9	248	55.9	18.5	4	672	34	18.3	15.8	37.3	0.640	1188
		2	1379	6	8.2	109	36.9	61.1	20.8	367	47.3	40.9	2.3	151	0.670	893
	Deep wells	3	1467	151	7.7	120	27.7	19.3	4.8	400	16.2	7.5	5.4	5.4	0.020	653

The model for the north-eastern flank (Fig. 2) suggests that there is an influence of the volcanic gases in the groundwater chemistry of the two hydrothermal springs (S42 and S43). The waters that have undergone deep infiltration in the high-altitude recharge area came in contact with a deep magmatic source, before flowing back to the surface along a fracture. The fracture is directly connecting the deep magmatic source to the groundwater discharged in the

hydrothermal springs. The volcanic gases also may diffuse to much lower extent, affecting the deep circulating waters in a regional flow system. The two springs from the discharge area (S18 and STP6), are attributed to be the discharge of the regional flow system, that have been affected by the volcanic gases (Bennett et al., 2021). The models suggest that there are two different local flow systems; the upstream-downstream evolution of the springs (which are on a shallow flow line) and the evolution in some lowermost shallow wells, which are clearly locally recharged, as shown by their lower mineralisation (compared to the upstream) and sometimes also anthropogenic pollution (Bennett et al., 2021); this is observed on the northern flank of Ngurdoto crater (Fig. 3) and on the south-western flank of Mount Meru (Fig. 5). The upstream-downstream evolution of the shallow wells (except the lowermost ones) is showing an intermediary flow system, whereas the deep wells are in a regional flow system (Fig. 5). The mixture of water from different flow systems is seen in wells W100 and W101 (Fig. 5), where the regional flow system (deep circulating waters) and shallow flow system (shallow flow waters) are discharging together.

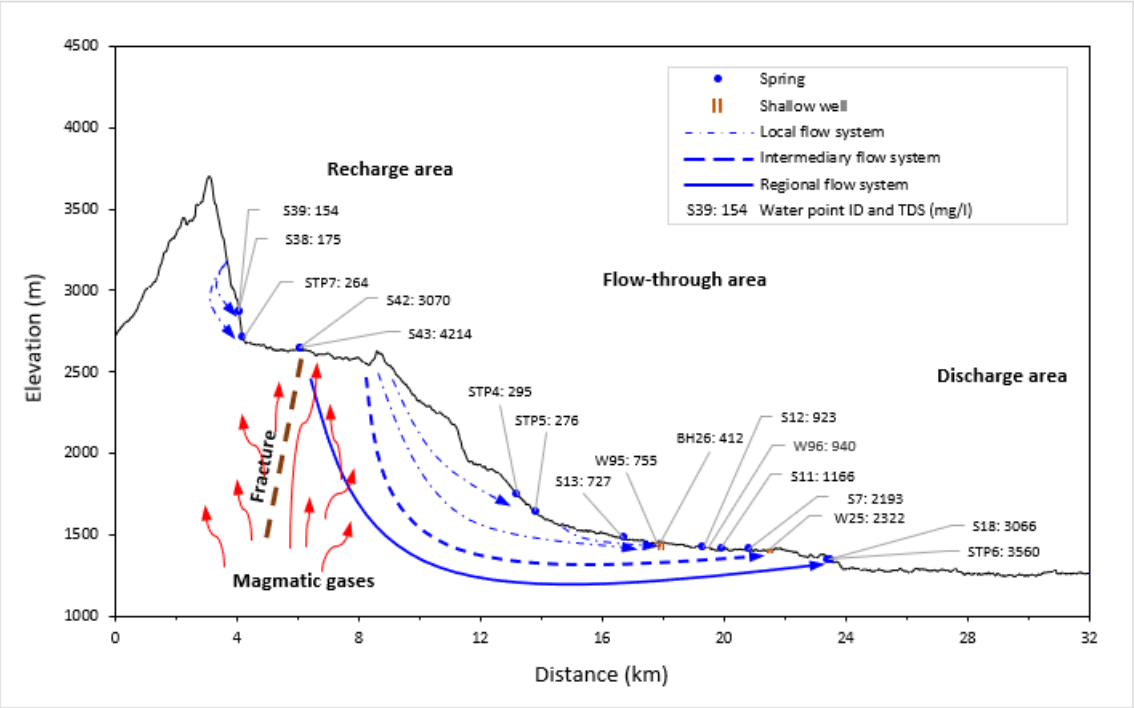

Fig. 2. Simplified groundwater flow conceptual model for the north-eastern flank of Mount Meru adapted from Bennett et al. (2021), suggesting the influence of the volcanic gases in the groundwater chemistry and also showing the increase of groundwater mineralisation with water residence times.

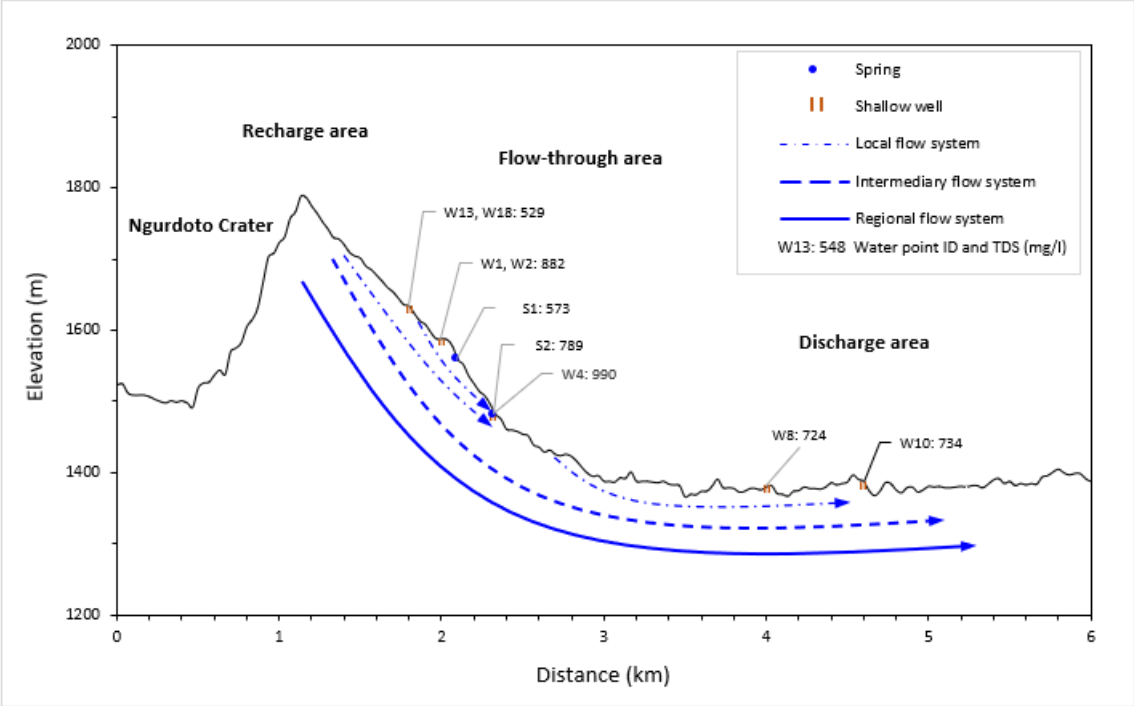

196

197 **Fig. 3.** Simplified groundwater flow conceptual model for the northern flank of Ngurdoto crater
198 showing the increase of groundwater mineralisation with water residence times.

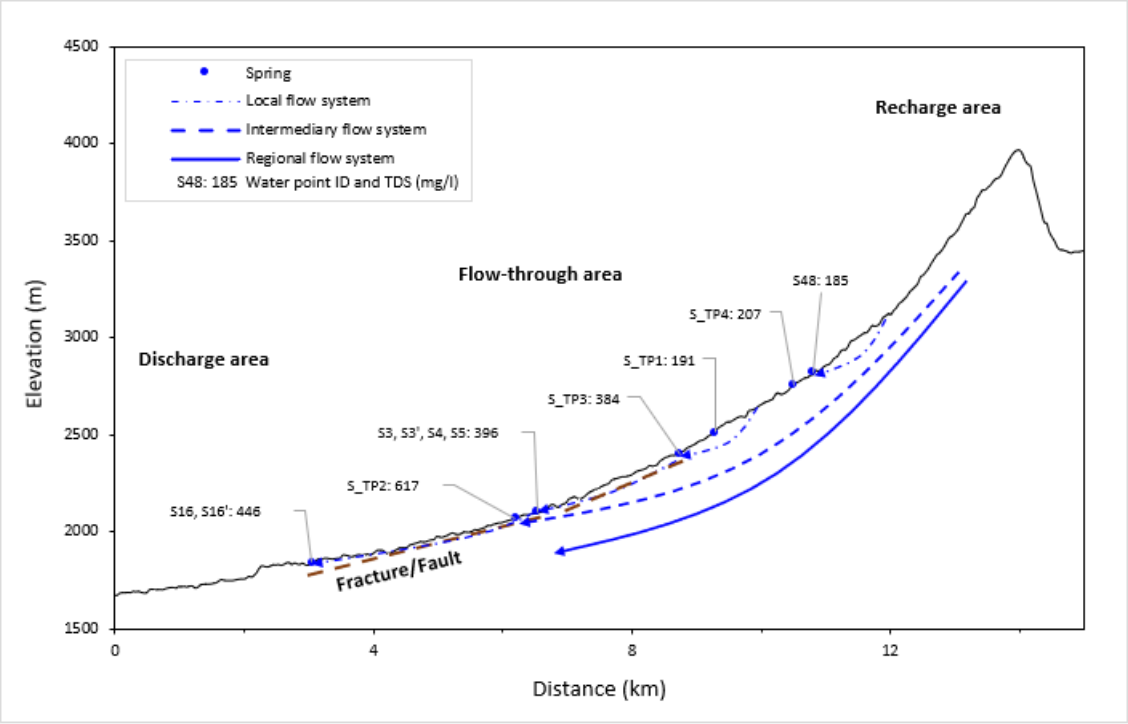

199

200 **Fig. 4.** Simplified groundwater flow conceptual model for the north-western flank of Mount
201 Meru showing the increase of groundwater mineralisation with water residence times.

202

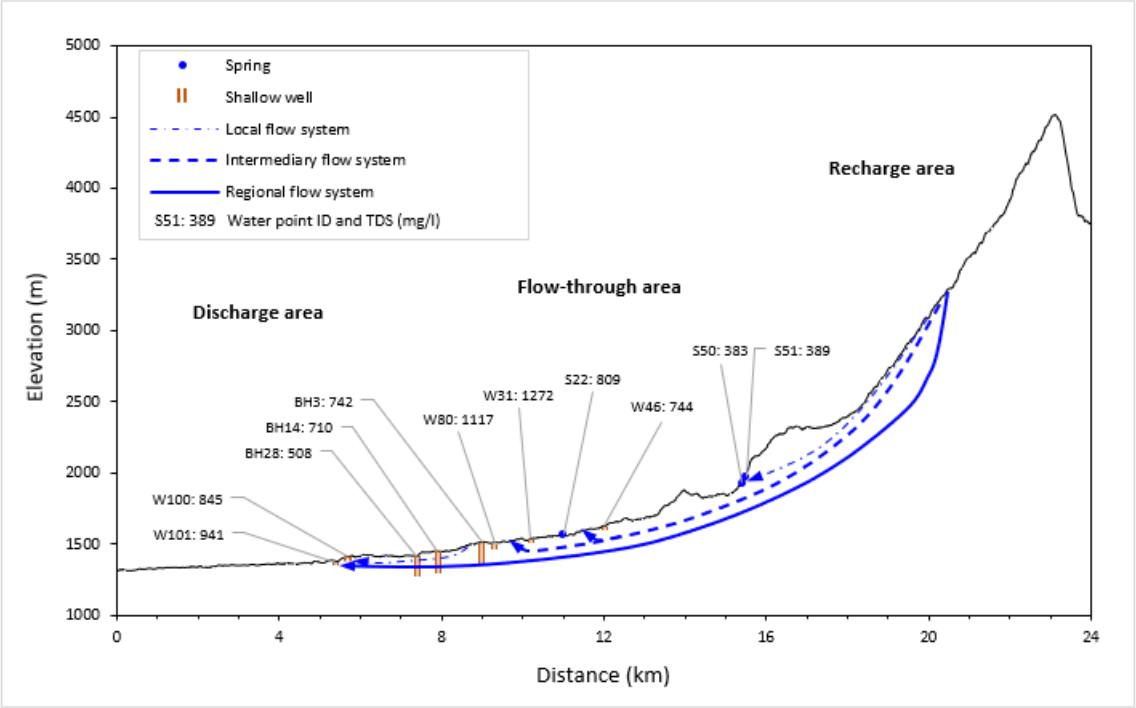

Fig. 5. Simplified groundwater flow conceptual model for the south-western flank of Mount Meru showing the increase of groundwater mineralisation with water residence times.

3.2. Equilibrium status of groundwater

3.2.1. Mineral saturation states and partial pressure of $CO_{2(g)}$

Fig. 6 a to b show saturation index (SI) of potentially relevant minerals for the groundwater samples. Fig. 6a shows that the groundwater in the study area is undersaturated with respect to sulfate minerals (anhydrite and gypsum), halite (rock salt) and sylvite, indicating that the dissolution of sulfate minerals, rock salt and sylvite may be ongoing processes, provided that these minerals are present. However, Fig. 6b shows that the groundwater shows all three conditions; undersaturated, near equilibrium and oversaturated with respect to the carbonate minerals (aragonite, calcite, and dolomite), silica (chalcedony and quartz) and fluorite, this indicates that the dissolution and precipitation of these minerals may be ongoing processes, depending on the case. Fig. 7 shows the relationship between HCO_3^-+ CO_3^{2-} and logarithm of partial pressure of $CO_{2(g)}$ (log ($pCO_{2(g)}$)) for the groundwater samples. Most of the groundwater samples are in equilibrium with $CO_{2(g)}$ at values that correspond to $pCO_{2(g)}$ found in the soil zone. Two spring waters from the recharge area are very close to equilibrium with atmospheric $CO_{2(g)}$ ($pCO_{2(g)}=10^{-3.5}$ atm), this indicates the most quickly recharged waters. Five samples are in equilibrium with values above the common upper limit for $CO_{2(g)}$ in the soil zone ($pCO_{2(g)}=10^{-1.5}$ atm), this suggests the influence of $CO_{2(g)}$ from volcanic emissions. Their

$pCO_{2(g)}$ values range from $10^{-1.48}$ – $10^{-1.40}$ atm. These five water samples seem to correspond to waters with relatively low residence times as $HCO_3^- + CO_3^{2-}$ is relatively low compared to very high $pCO_{2(g)}$ since longer residence foster more weathering hence more $HCO_3^- + CO_3^{2-}$. The samples are from three springs (S11 (two samples), S12 and S17) and one shallow well (W32). S11 and S12 are bubbling springs (Fig. 8), located on the north-eastern flank. S17 and W32 are 375 m apart, located on the south-western flank. S17 is flowing laterally from a fractured less pervious layer.

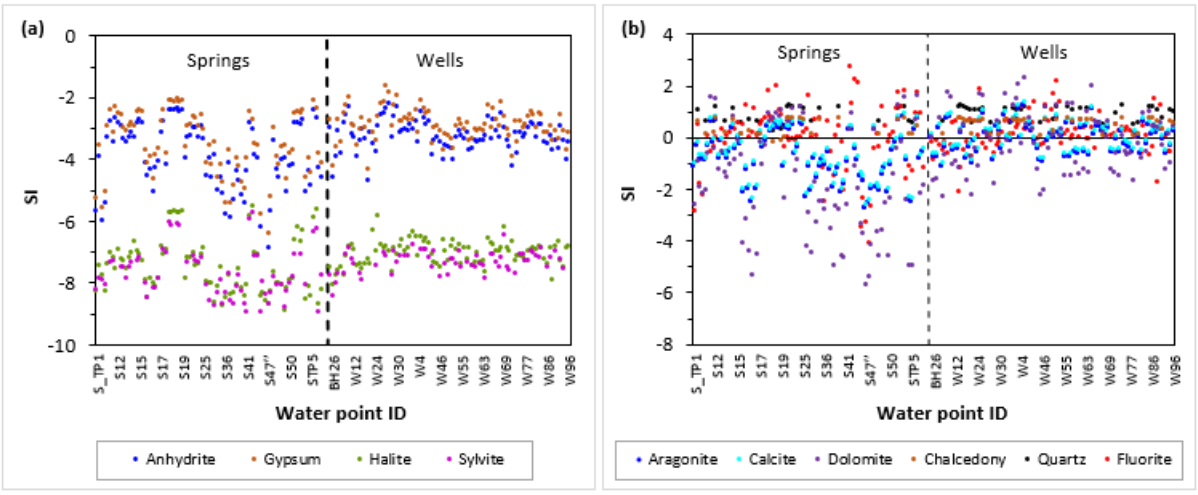

Fig. 6. a to **b**: Saturation index (SI) of potentially relevant minerals for the groundwater samples.

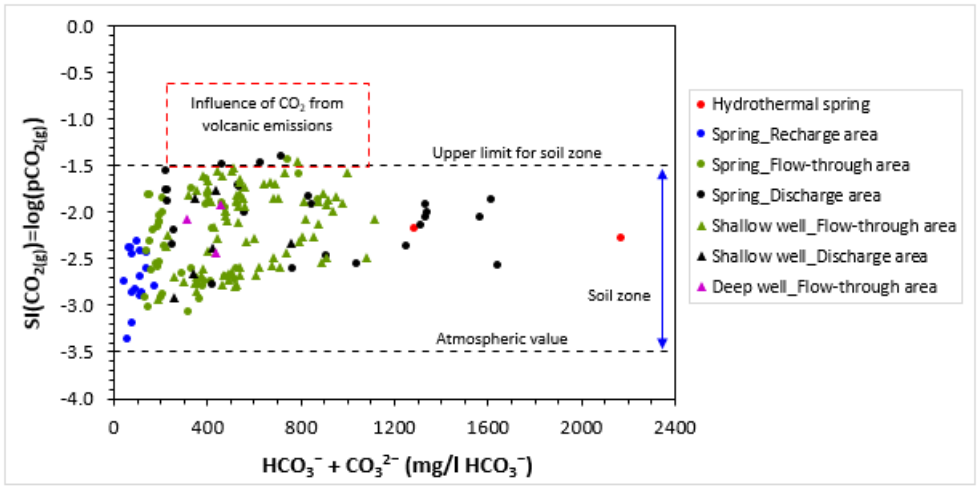

Fig. 7. Relationship between $HCO_3^- + CO_3^{2-}$ and log ($pCO_{2(g)}$) for the groundwater samples.

Fig. 8. Bubbling springs: (**a**) spring S11 and (**b**) spring S12.

3.2.2. Stability diagrams of silicate minerals

Fig. 9 a to c show the projections of all water samples in the stability diagrams for Na-, K-, and Ca-feldspars.

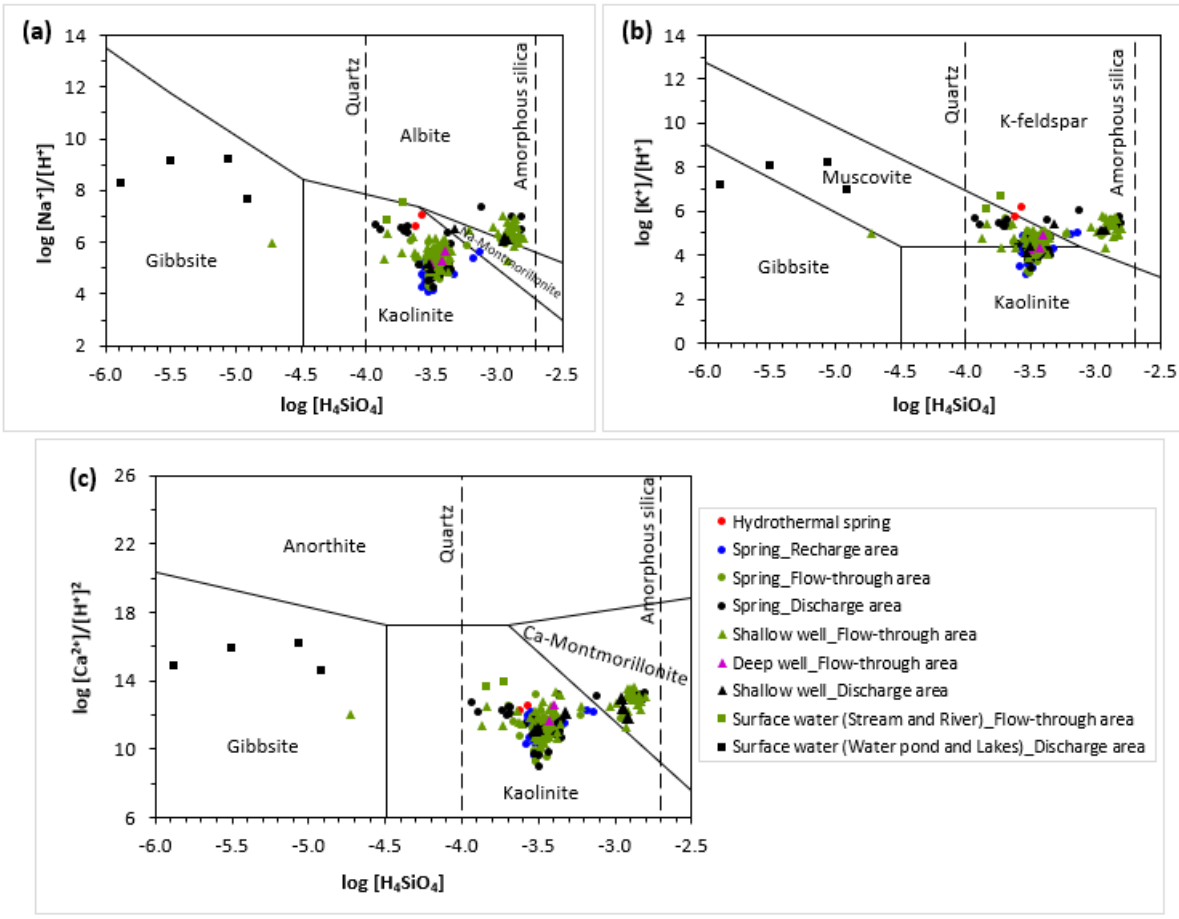

Fig. 9. a to **c**: Stability diagrams of Na-, K-and Ca-feldspars and its weathering products for groundwater samples from the study area. The dashed lines represent saturation with respect to quartz and amorphous silica.

Fig. 9a shows that the less mineralised groundwater samples (from recharge and flow-through areas which are more leached) lie within the kaolinite stability field while the more mineralised

ones (from flow-through and discharge areas that are less leached) lie within the albite stability field. Four surface water samples (1 from water pond and 3 from lakes) lie within the stability field of gibbsite, reflecting poor drainage conditions, and therefore stronger leaching (Walraevens et al., 2018), as both water pond and lakes are in closed basins: no water in, no water out. From the other two surface water samples, river water lies within the kaolinite stability field, while stream water lies at the boundary between kaolinite and albite stability fields, reflecting good drainage conditions. One water sample from a shallow well (24 m deep) lies within the stability field of gibbsite, the well went dry since May 2019 as observed during 2018–2020 groundwater level monitoring campaign, this suggests that the well was drawing water from a shallow perched aquifer with poor drainage conditions. Fig. 9b shows that the less mineralised groundwater samples lie within the stability field of kaolinite and muscovite while the more mineralised ones lie within the stability field of K-feldspar, whereas Fig. 9c shows that the less mineralised groundwater samples lie within the stability field of kaolinite while the more mineralised ones lie within the stability field of Ca-montmorillonite. All samples (except the five that lie within the stability field of gibbsite) fall to the right side of the quartz saturation line, indicating the groundwater is oversaturated with respect to quartz (the precipitation of which is kinetically inhibited in low-temperature systems), whereas they are undersaturated with respect to amorphous silica as all samples fall to the left side of the amorphous silica saturation line; thus amorphous silica will dissolve.

3.3. Hydrogeochemical processes controlling groundwater chemistry

Petrographic observations of rock samples for this study show that clinopyroxene (content: 20-40%), nepheline (content: 10-30%), ilmenite/magnetite (content: 5-10%) and sanidine (found in few samples, content: 15-30%) are important minerals. Biotite is found in minor amount (content: 1%) (M Kisaka 2020, unpublished data). Augite, which is the most common clinopyroxene, and anorthoclase that contains albite and sanidine were reported as important minerals in the area by Ghiglieri et al. (2012). Since anorthoclase is a solid solution, consisting of 64-90% of albite ($NaAlSi_3O_8$) and 10-36% of orthoclase ($KAlSi_3O_8$) (or its high-temperature form sanidine), albite is the dominant form of alkali feldspar found in the study area. Augite is mostly composed of diopside ($CaMgSi_2O_6$) and hedenbergite ($CaFeSi_2O_6$), but the diopside is the most significant clinopyroxene end member and is going to be used for the dissolution reaction in this study.

The common natural sources for forming F^--rich groundwater include dissolution of natural F^--bearing minerals (such as amphibole, biotite, fluorapatite and fluorite) (Ghiglieri et al.,

2012; Luo et al., 2018) and magmatic degassing related to volcanic activity (Sawyer et al., 2008; Jasim et al., 2018). Calcite precipitation, cation exchange, salinization and evaporation are important hydrogeochemical processes that allow for increasing F^- concentrations by reducing the Ca^{2+} concentrations in groundwater (Nanyaro et al., 1984; Coetsiers et al., 2008; Luo et al., 2018). The F^--bearing minerals found in the study area are amphibole, biotite and fluorapatite (Ghiglieri et al., 2012; M Kisaka 2020, unpublished data). However, the exact abundance and chemical composition of these minerals including their F^- contents are unknown. In our data, the F^-/Cl^- ratio of 98% (n=172) of the groundwater samples is > 0.10 while only 2% (n=3) of the samples have F^-/Cl^- < 0.10, indicating that the F^- in the groundwater in the study area is derived from the chemical weathering of rock minerals (Kilham and Hecky, 1973).

Table 2 shows the dissolution reactions for the important minerals found in the study area. Theoretically, the weathering of albite to kaolinite releases Na^+ and HCO_3^- in the equivalent ratio of 1:1 whereas the weathering of sanidine to kaolinite releases HCO_3^- and K^+ in the equivalent ratio of 1:1. The weathering of nepheline to kaolinite releases Na^+ and HCO_3^- in the equivalent ratio of 4:3 and HCO_3^- and K^+ in the equivalent ratio of 4:1. The weathering of diopside releases HCO_3^- and Ca^{2+} in the equivalent ratio of 4:1 and HCO_3^- and Mg^{2+} in the equivalent ratio of 4:1. The weathering of biotite to kaolinite releases HCO_3^- and K^+ in the equivalent ratio of 3:1, HCO_3^- and Mg^{2+} in the equivalent ratio of 3:2, F^- and K^+ in the equivalent ratio of 1:1 and F^- and Mg^{2+} in the equivalent ratio of 1:2. The weathering of fluorapatite releases HCO_3^- and Ca^{2+} in the equivalent ratio of 6:5 and F^- and Ca^{2+} in the equivalent ratio of 1:5.

Table 2. Dissolution reactions of the important minerals found in the study area

$2NaAlSi_3O_8 + 9H_2O + 2H_2CO_3 \leftrightarrow Al_2Si_2O_5(OH)_4 + 2Na^+ + 2HCO_3^- + 4H_4SiO_4$ Albite Kaolinite
$2KAlSi_3O_8 + 9H_2O + 2H_2CO_3 \leftrightarrow Al_2Si_2O_5(OH)_4 + 2K^+ + 2HCO_3^- + 4H_4SiO_4$ Sanidine Kaolinite
$Na_3KAl_4Si_4O_{16} + 2H_2O + 4H_2CO_3 \leftrightarrow 2Al_2Si_2O_5(OH)_4 + 3Na^+ + K^+ + 4HCO_3^-$ Nepheline Kaolinite
$CaMgSi_2O_6 + 4CO_2 + 6H_2O \leftrightarrow Ca^{2+} + Mg^{2+} + 4HCO_3^- + 2H_4SiO_4$ Diopside
$2KMg_2FeAlSi_3O_{10}(FOH) + 9H_2O + 6H_2CO_3 \leftrightarrow Al_2Si_2O_5(OH)_4 + 2K^+ + 4Mg^{2+} + 2F^- + 6HCO_3^- + 2Fe(OH)_3 + 4H_4SiO_4$ Biotite Kaolinite
$Ca_5(PO_4)_3F + 6CO_2 + 6H_2O \leftrightarrow 5Ca^{2+} + 3H_2PO_4^- + F^- + 6HCO_3^-$ Fluorapatite

3.3.1. Dissolution of weathering aluminosilicate minerals

EC show significant very strong positive monotonic correlations with $HCO_3^- + CO_3^{2-}$ (Fig. 10a) and Na^+ (Fig. 10b), a significant strong positive monotonic correlation with K^+ (Fig. 10c) and significant moderate positive monotonic correlations with Mg^{2+} (Fig. 10d) and Ca^{2+} (Fig. 10e). The EC reflects the salinity or the mineralisation of groundwater, hence high values of EC indicate mature waters with long residence times which have dissolved the maximum of rock-forming materials (Walraevens et al., 2018). Thus, the EC in our study area reflects the extent of weathering and dissolution of aluminosilicate minerals, and the contribution of other processes such as calcite precipitation, the evaporative concentration, the dissolution of evaporitic salts and anthropogenic pollution. The dissolution of weathering aluminosilicate minerals leads to the addition of cations and silica as well as the increase of pH resulting from the consumption of acid (Walraevens et al., 2018). The positive correlation of EC with the total alkalinity ($HCO_3^- + CO_3^{2-}$) indicates the increasing release of HCO_3^- as a result of the increasing dissociation of H_2CO_3. The positive correlations of EC with alkaline elements (Na^+ and K^+) and alkaline earth elements (Ca^{2+} and Mg^{2+}) indicates the progressive increase of these ions with the mineralisation of the groundwater, in response to the dissolution of weathering aluminosilicate minerals and other hydrogeochemical processes. The strong correlation of EC with alkaline elements (Na^+ and K^+) and moderate correlation with alkaline earth elements (Ca^{2+} and Mg^{2+}) suggests the significant contribution of Na-K-bearing minerals in releasing cations in the groundwater, and much less of Ca-Mg-bearing minerals.

Fig. 11 shows that the dissolution of albite (alkali feldspar) controls groundwater chemistry in the area because most samples plot along the 1:1 line (Fig. 11a). This dissolution determines the bicarbonate concentration in the groundwater, while the other cations show a deficit compared to HCO_3^- (Fig. 11b-d). The dissolution of diopside releases Ca^{2+} since all samples

plot above the line representing weathering of diopside (4:1 line) (Fig. 11c). Besides, at high concentrations, HCO_3^- starts to show a deficit compared to Na^+ (deviation from the 1:1 line) (Fig. 11a), which is due to calcite precipitation (the Ca^{2+} provided by diopside) at high concentrations. Fig. 12 confirms the precipitation of calcite at high HCO_3^- concentrations (supersaturated waters) in the study area. It is interesting to note that Jasim et al. (2018) mention that chemical precipitation may lead to plugging in areas of intense mineralisation, which may cause increasing pore pressures and flank collapse. The collapsed flank of Mount Meru coincides with the area where the hydrothermal springs are found, and where mineralisation is the highest. Ingebritsen et al. (2010) state that such increasing pore pressures may cause violent steam-driven explosions. The glass phase of the volcanic rocks, which is volumetrically dominant, structurally amorphous (so potentially easier to dissolve) and has a composition that is not all that different from the alkali feldspar, may also contribute to the groundwater chemistry. The dissolution of sanidine, biotite and nepheline releases K^+ as all samples plot above the lines representing weathering of sanidine (1:1 line), biotite (3:1 line) and nepheline (4:1 line) (Fig. 11b), whereas the dissolution of biotite and diopside releases Mg^{2+} as all samples plot above the lines representing weathering of biotite (3:2 line) and diopside (4:1 line) (Fig. 11d).

The saturation indices (SI) of calcite in groundwater samples (Fig. 12) represent undersaturated ($SI < 0$), equilibrium ($SI = 0$) and oversaturated ($SI > 0$) conditions. The dissolution of calcite (which is expected to occur when $SI < 0$) is an insignificant process in the study area since carbonate minerals are not found in the main geological formations. They are only found in the crusts of lake deposits, and in breccias and calcrete on mantling ash deposits (Ghiglieri et al., 2012). Therefore, the precipitation of calcite occurring in the oversaturated samples ($SI > 0$) indicates that this mineral is present as a secondary product. It is produced due to following reactions: the dissolution of $CO_{2(g)}$ which forms H_2CO_3 causes extensive aluminosilicate dissolution, raising the pH and HCO_3^- in the groundwater; at pH=8.2, the HCO_3^- transforms to CO_3^{2-} which reacts with the available Ca^{2+} to form calcite ($CaCO_3$). As the chemical reactions progress and calcite becomes oversaturated in the system, it will precipitates.

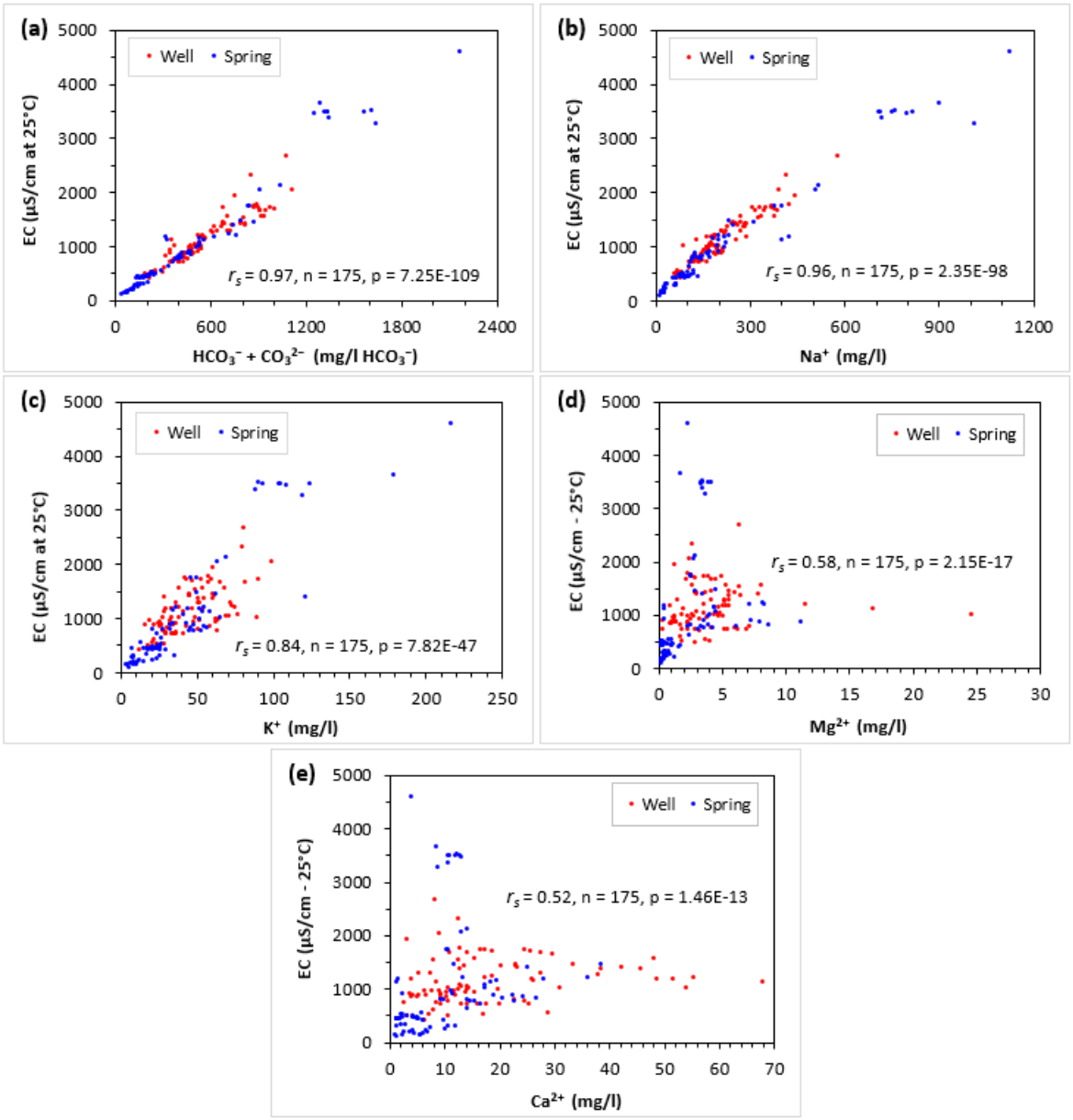

Fig. 10. a to **e**: Bivariate plots of EC versus HCO_3^- + CO_3^{2-} and major cations.

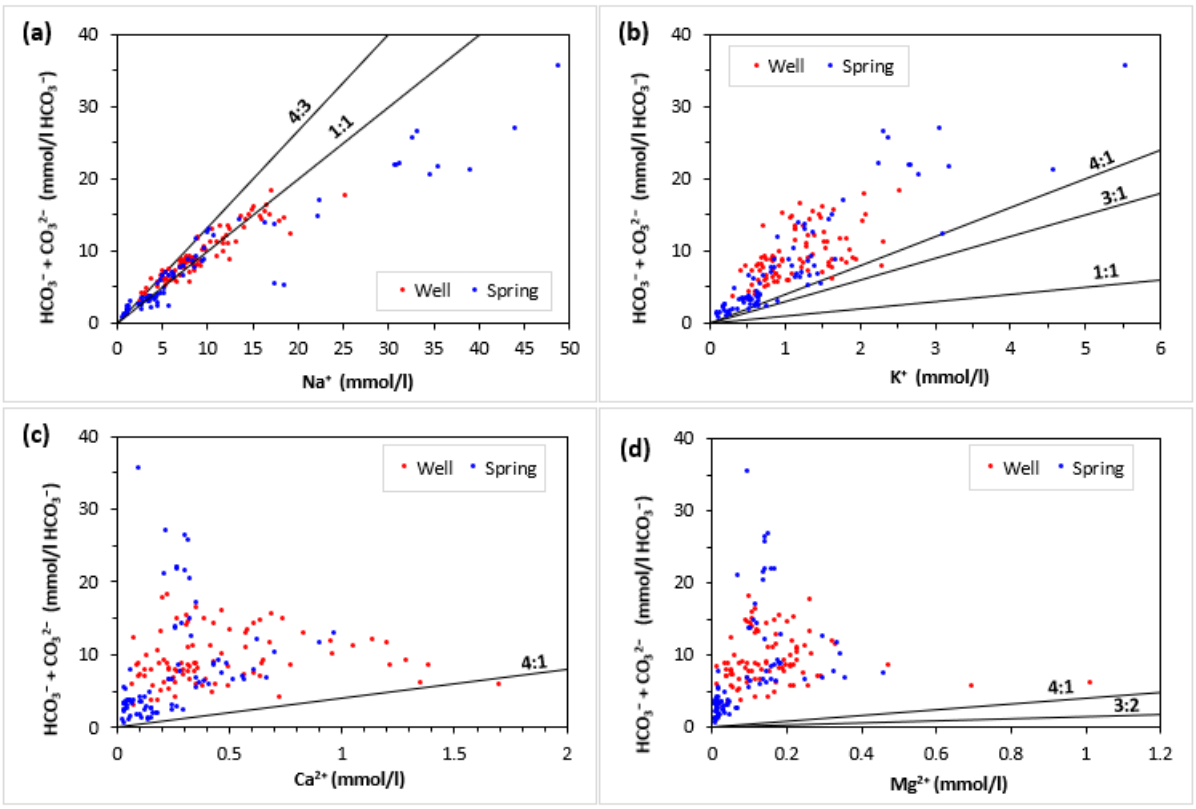

Fig. 11. **a** to **d**: Bivariate plots of $HCO_3^- + CO_3^{2-}$ versus major cations. Black lines represent the theoretical dissolution curves of the important minerals found in the study area (Table 8).

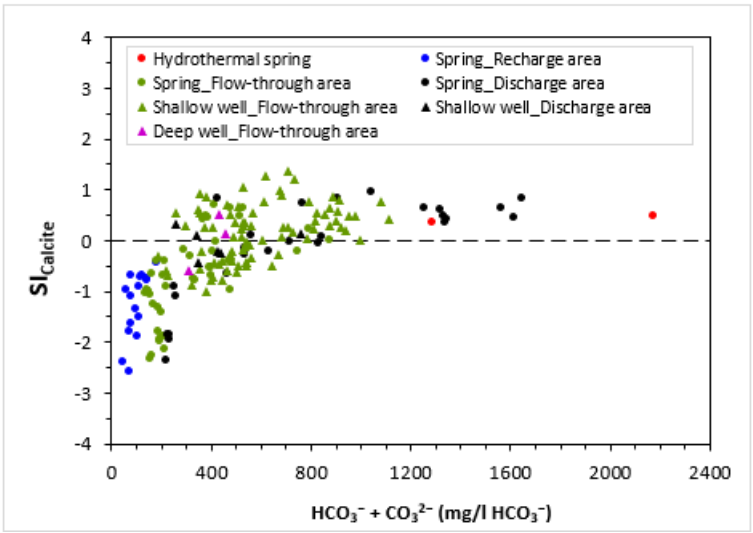

Fig. 12. Bivariate plot of saturation index (SI) of calcite versus $HCO_3^- + CO_3^{2-}$ in groundwater samples.

3.3.2. Dissolution of fluoride-bearing minerals

Fig. 13 shows that the F^- concentration in the groundwater is progressively increasing together with the mineralisation of the groundwater (increasing in TDS) along the flow paths, in response to the dissolution of fluoride-bearing minerals and other hydrogeochemical processes.

F^- concentration in the groundwater shows significant moderate positive correlations with Na^+ and HCO_3^-+ CO_3^{2-}, and a significant weak positive correlation with K^+ (Bennett et al., 2021), suggesting that the dissolution of weathering Na-K-bearing minerals increases pH in the groundwater, which in turn activates the dissolution of $CO_{2(g)}$, and finally leads to the precipitation of calcite as secondary product (see *section 3.3.1*). The precipitation of calcite as a secondary product lowers the Ca^{2+} concentration in the groundwater and leads to sub-saturation with respect to fluorapatite ($Ca_5(PO_4)_3F$); hence fluorapatite, whenever present, dissolves and releases F^- to the system. This is supported by the weak negative monotonic correlation between F^- and Ca^{2+}: as the groundwater chemical processes progress, the groundwater becomes highly enriched in F^- concentrations with lower Ca^{2+} concentrations (Coetsiers et al., 2008; Hu et al., 2013; Wu et al., 2015; Kumar et al., 2017; Luo et al., 2018).

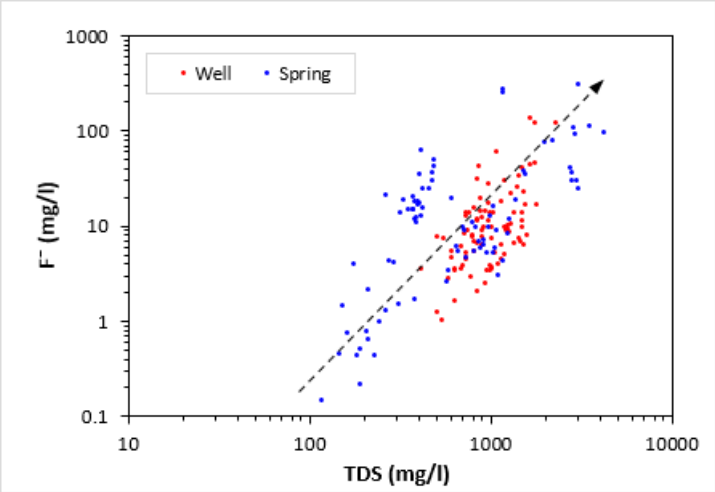

Fig. 13. Bivariate plot of F^- versus TDS in groundwater samples.

Fig. 14a shows that few samples plot along the 1:1 line representing the dissolution of biotite. The samples above the line indicate the surplus of F^- from fluorapatite, other fluoride-bearing minerals and volcanic gases, whereas the samples below the line indicate the surplus of K^+ resulting from the dissolution of weathering aluminosilicate minerals. A sample from one hydrothermal spring plots along 1:1 line, and this is consistent with the dissolution of biotite. The sample from the other hydrothermal spring plots above the line, suggesting the contribution from volcanic gases. Fig. 14b shows that few samples plot along the 1:2 line representing the dissolution of biotite while most of the samples plot above the line. The same is observed on Fig. 14c where few samples plot along the 1:5 line representing the dissolution of fluorapatite while most of the samples plot above the line, including spring water samples from the recharge areas. The springs from the recharge areas are all undersaturated with respect

to calcite (Fig. 12) and dolomite (Fig. 15). Therefore, all should lie along the 1:2 line in Fig. 14b and along the 1:5 line in Fig. 14c to be consistent with the dissolution of biotite and fluorapatite respectively, which is not the case. Thus, the surplus of F^- in these springs is a clear indication to the contribution from the volcanic gases. For highly mineralised samples, this is less clear, as the calcium deficit may be due to calcite precipitation.

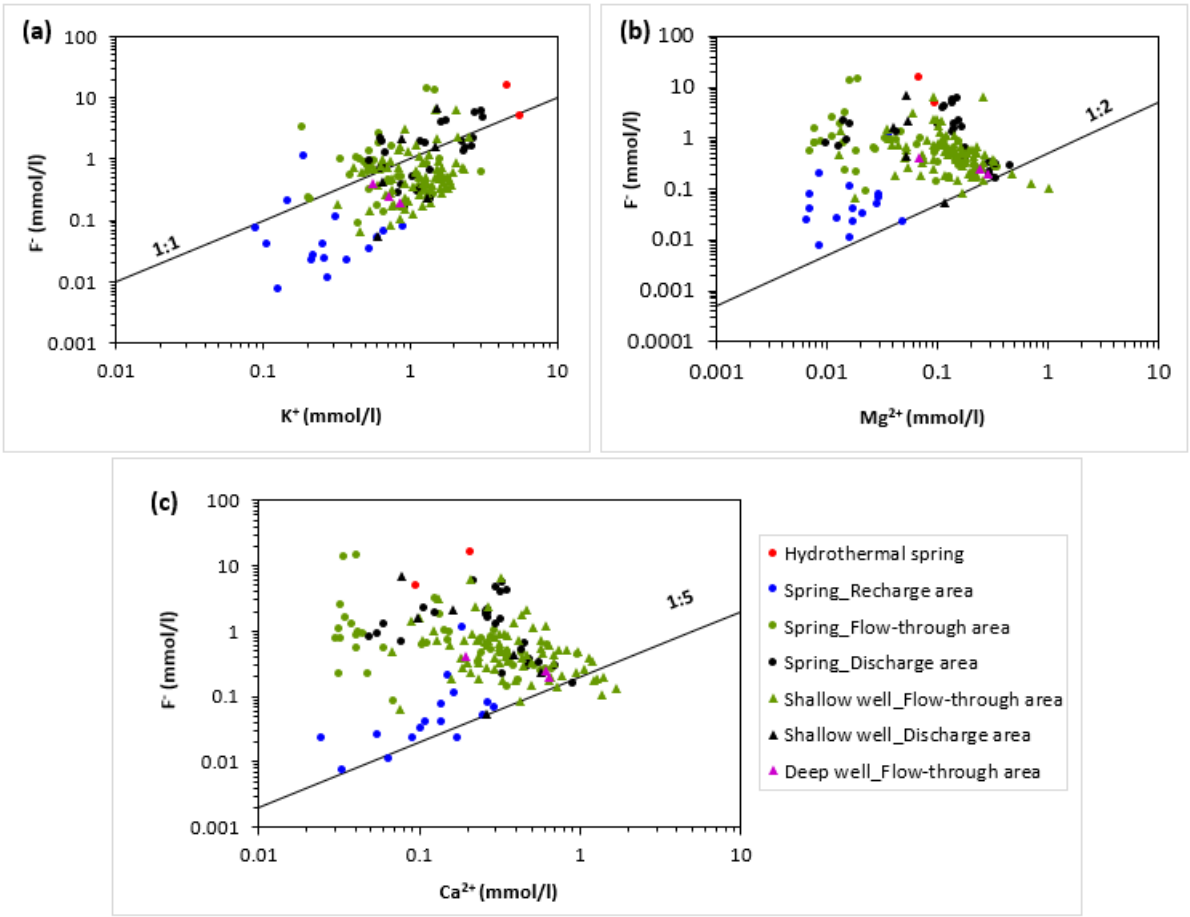

Fig. 14. a to **c**: Bivariate plots of F^- versus Ca^{2+}, K^+ and Mg^{2+} in groundwater samples. Black lines represent the theoretical dissolution curves of biotite and fluorapatite (Table 2).

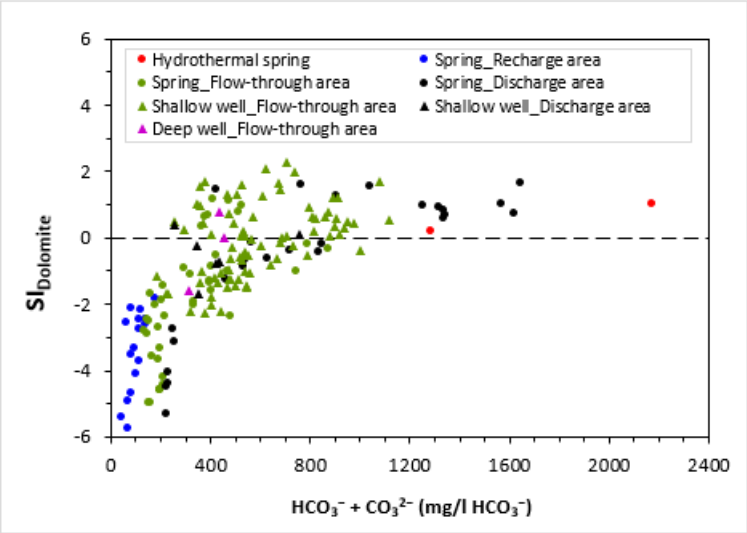

Fig. 15. Bivariate plot of saturation index (SI) of dolomite versus HCO_3^- + CO_3^{2-} in groundwater samples.

3.3.3. Dissolution of volcanic gases

Significant fumarolic activity was recorded in the Ash Cone area from 1910 (Mount Meru's last eruption) until 1954 CE (Wilkinson et al., 1983). However, no measurements were done to know what gases were exsolving from the magma. The two hydrothermal springs located just at the foot of the Ash cone show high values of alkalinity, SO_4^{2-}, Cl^- and F^- compared to the surrounding springs (Bennett et al., 2021), this suggests the influence of the admixture of volcanic gases: CO_2, SO_2, HCl and HF from depth (Sawyer et al., 2008; Jasim et al., 2018). This same activity can be expected to also affect much of the other groundwater, be it in a much weaker measure. The volcanic gases that are already in the subsoil are transformed into dissolved $CO_{2(g)}$, SO_4^{2-}, Cl^- and F^-. By considering SO_4^{2-}, Cl^- and F^- as tracers to determine the influence of the volcanic gases in the groundwater chemistry in the study area, the correlation of these ions was analysed. Results show significant strong positive correlation between SO_4^{2-} and Cl^-, and significant weak positive correlations of F^- with Cl^- and SO_4^{2-} (Bennett et al., 2021). This suggests the influence volcanic emissions at depth. The influence of $CO_{2(g)}$ from volcanic emissions is noticed in the five samples which are in equilibrium with $CO_{2(g)}$ at values that are above the common upper limit for $CO_{2(g)}$ in the soil zone (see *section 3.2.1*).

The discussion of hydrochemical parameters and their spatial distribution (Bennett et al., 2021), the mineral saturation status, and the stability of Na-, K-, and Ca-feldspars have allowed to indicate hydrogeochemical processes controlling groundwater chemistry in the study area. The main processes are the dissolution of weathering aluminosilicate minerals, dissolution of F^--

bearing minerals, precipitation of carbonate minerals and dissolution of volcanic gases. Evaporative concentration of solutes, precipitation and redissolution of evaporitic salts may locally play a role as they take place only at/near the surface.

3.4. Spatial distribution of fluoride concentration with relation to the geological units

Fig. 1 shows the spatial distribution of F^- concentrations in different geological formations in the study area. The spatial distribution is further analysed and discussed in six groups based on the six clusters of the inventoried water points discussed in *section 2.2*.

3.4.1. Eastern flank

Table 3 summarises some descriptive statistics of F^- and TDS values in water samples from different geological formations and different flow system zones in the eastern part of the Arusha National Park. The flow system consists of the recharge area, flow-through area, and discharge area. In this study, these areas have been categorised based on elevation, slope, spring settings and groundwater level. The springs from the recharge areas located in the pyroclastics with subordinate nephelinitic and phonolitic lavas and in the Momella DAD show lower mineralisation (average TDS: 213 and 190 mg/L respectively) and lower F^- values (average 1.5 and 0.8 mg/L respectively) compared to other water sources, indicating young spring waters. The springs are at higher elevations at the centre of Mount Meru where there are steep slopes and lower temperatures. Steep slopes in this area lead to shorter water residence times while lower temperatures hinder the enrichment of F^- due to slow weathering and dissolution of aluminosilicate minerals, hence lower F^- values are observed. The spring from the recharge area located in the lake deposits near the Ash cone shows relatively high TDS and F^- values (264 and 21.4 mg/L respectively) compared to the former ones, suggesting that the fine silty lake deposits are highly weatherable and readily dissolve in water compared to the pyroclastics, lava flows and DADs. The two hydrothermal springs (the Njekukumia springs) from the recharge area located in the porous pyroclastics with nephelinitic and phonolitic lavas provide an exception, as they are highly mineralised (average TDS: 3642 mg/L) with high F^- values (average: 198 mg/L). They are also warmer (average temperature: 20.0°C) than the surrounding springs (average temperature: 13.3°C), indicating they are from a deeper source, thus their high temperature and longer residence times lead to their higher mineralisation and higher F^- values. In the flow-through area in the Momella DAD, two water samples from the Tululusia springs (S44 and S45) show significant mineralisation (average TDS: 1174 mg/L) with high F^- values (average: 264 mg/L), indicating progressive mineralisation of the groundwater along the flow paths due to long water residence times and high rock weatherability, in addition to the

471 influence of the volcanic gases. The mineralisation and high F^- values of the Tulusia springs
472 might be influenced by the infiltrated hydrothermal spring water as suggested by Bennett et al.
473 (2021). Also, in the flow-through area in the Momella DAD, the sample from the Njekukumia
474 stream shows high TDS and F^- values: 3540 and 553 mg/L respectively. These high values are
475 attributed to one of the hydrothermal springs, the Small Njekukumia spring (S42), which shows
476 high TDS and F^- values: 3070 and 301 mg/L respectively. Water samples from the three closed
477 basin lakes located in the discharge area show the highest mineralisation (average TDS: 13541
478 mg/L) and highest F^- values (average: 736 mg/L), indicating mature surface waters with longer
479 residence times and high evaporative concentration of solutes. On the eastern flank, the young
480 spring waters from the recharge areas at higher elevations at the centre of Mount Meru,
481 emerging from the pyroclastics (with subordinate nephelinitic and phonolitic lavas) and from
482 the Momella DAD, have F^- not exceeding the WHO limit, and are suitable as healthy drinking
483 water.

484 **Table 3.** Descriptive statistics of F^- and TDS values in the water samples from different
485 geological formations and different flow system zones on the eastern part of the Arusha
486 National Park (n: number of samples).

Geological formation	Zone	Water source	n	Average elevation (m)	F^- (mg/l)		Average TDS (mg/l)
					Range	Mean	
Pyroclastics with subordinate nephelinitic and phonolitic lavas	Recharge area	Springs	6	2427	0.4 - 3.9	1.5	213
		Hydrothermal springs	2	2527	95.2 - 301	198	3642
lake deposits	Recharge area	Spring	1	2630		21.4	264
Momella DAD	Recharge area	Springs	6	2206	0.1 - 2.1	0.8	190
	Flow-through area		3	1780	14.9 - 274	181	899
	Flow-through area	Stream	1	2132		553	3540
	Discharge area	Lakes	3	1430	217 - 1004	736	13541

487
488
489 On the northern flank of Ngurdoto crater, all water samples are from the Momella DAD. Table
490 4 shows that water samples from Nkoasenga show the increase of F^- values along the flow path
491 along with the progressive mineralisation of the groundwater. In the flow-through areas, wells
492 and springs show similar mineralisation, and this can be attributed to comparable residence
493 times. The shallow wells in Leguruki show similar TDS and F^- values as shallow wells and
494 springs in the flow-through areas in Nkoasenga. The low mineralisation and low F^- values of
495 these wells compared to the shallow wells in the discharge area in Nkoasenga are attributed to
496 the shorter water residence times, and so these are waters from the local flow system (see Fig.
497 3). On this flank, shallow wells from the flow-through area (see Fig. 3) provide groundwater

498 with F^- (mostly) below Tanzanian limit (average: 3.5 mg/L). In Leguruki in the regional
499 discharge area, a local flow system results in F^- levels that are still reasonable (average: 4.6
500 mg/L).

501 **Table 4.** Descriptive statistics of F^- and TDS values in the water samples from different
502 geological formations and different flow system zones on the northern flank of Ngurdoto crater.

Region	Geological formation	Zone	Water source	n	Average elevation (m)	Average well depth (m)	F^- (mg/l)		Average TDS (mg/l)
							Range	Mean	
Nkoasenga	Momella DAD	Flow-through area	Shallow wells	7	1586	8	1.3 - 7.4	3.5	605
			Springs	2	1522		2.6 - 10.7	6.7	681
		Discharge area	Shallow wells	3	1491	12	30.7 - 134	68.6	1118
			Water pond	1	1429			85.9	3237
Leguruki	Momella DAD	Discharge area	Shallow wells	3	1354	8	1.0 - 8.2	4.6	666

503
504

505 ### *3.4.2. North-eastern flank*

506 Table 5 shows the descriptive statistics of F^- and TDS values in the water samples from the
507 north-eastern flanks of Mount Meru: Mkuru, Uwiro and Ngarenanyuki. At higher elevations,
508 samples from the flow-through areas, i.e. two springs located in the pyroclastics and associated
509 lavas and one shallow well located in the lake deposits, show low mineralisation and low F^-
510 values, which is attributed to their short residence times. In the lake deposits, springs from the
511 discharge area are more mineralised with high F^- values compared to a shallow well in the
512 flow-through area at slightly higher elevation, indicating progressive mineralisation of the
513 groundwater along the flow paths with increasing residence times. The samples from the flow-
514 through area in the Engosomit DAD, alkaline parasitic cone and alluvial fan deposits and those
515 from the discharge area in the lake deposits show similar intermediate mineralisation with high
516 F^- values, suggesting comparable long residence times. The progressive mineralisation of the
517 groundwater along the flow paths with increasing residence times is also observed in the
518 Momella DAD: the samples from the discharge area are highly mineralised with high F^- values
519 compared to those from the flow-through area. The higher F^- value in the Ngarenanyuki river
520 is primarily attributed to the hydrothermal spring water via the Njekukumia stream (Bennett et
521 al., 2021). On this flank, springs and shallow wells from the flow-through area on pyroclastics
522 (and associated lavas) and lake deposits, deliver water with relatively low F^- (3.6–4.3 mg/L),
523 which could be used for mixing with low F^- water, to produce drinking water with F^- below
524 Tanzanian limit.

Table 5. Descriptive statistics of F^- and TDS values in the water samples from different geological formations and different flow system zones on the north-eastern flank of Mount Meru.

Geological formation	Zone	Water source	n	Average elevation (m)	Average well depth (m)	F^- (mg/l)		Average TDS (mg/l)
						Range	Mean	
Pyroclastics (stippled) and associated lavas	Flow-through area	Spring	1	1726			4.2	295
Pyroclastics (stippled) and associated lavas covered with mantling ash	Flow-through area	Spring	1	1684			4.3	276
lake deposits	Flow-through area	Shallow well	1	1551	48		3.6	412
	Discharge area	Springs	8	1415		3.0 - 12.5	6.8	993
Engosomit DAD	Flow-through area	Shallow well	1	1520	23		9.1	755
Alkaline parasitic cone	Flow-through area	Springs	5	1452		6.2 - 15.8	10.0	793
Alluvial fan deposits	Flow-through area	Shallow wells	6	1443	6	13.6 - 30.1	18.3	931
Momella DAD	Flow-through area	Shallow wells	4	1427	10	11.7 - 121	43.3	1223
		River	1	1443			144	1544
	Discharge area	Springs	12	1360		24.9 - 113	58.0	2595

3.4.3. North-western flank

On the north-western flank, in Oldonyo Sambu, the springs from the recharge area are in the pyroclastics with subordinate nephelinitic and phonolitic lavas, whereas the springs from the flow-through and discharge areas are in the Lemurge DAD. The recharge area is at higher elevation whereas the flow-through area is at intermediate elevation and the discharge area at lower elevation. Table 6 shows that the springs from the recharge area show low mineralisation with lower F^- values, due to the slow weathering and dissolution of aluminosilicate minerals and short water residence times, whereas the springs from the flow-through and discharge areas show high F^- values due to the progressive mineralisation of the groundwater along the flow paths. On average, the springs from the flow-through and discharge areas show similar mineralisation with comparable F^- values, due to shorter residence times as the groundwater is flowing through fractures between the two flow zones (see Fig. 4). On the northwestern flank, springs on higher elevations in the recharge area, emerging from pyroclastics (with lavas) deliver excellent quality water with F^- below WHO-limit (average 0.6 mg/L).

Table 6. Descriptive statistics of F^- and TDS values in the water samples from different geological formations and different flow system zones on the north-western flank of Mount Meru.

Geological formation	Zone	Water source	n	Average elevation (m)	F^- (mg/l)		Average TDS (mg/l)
					Range	Mean	
Pyroclastics with subordinate nephelinitic and phonolitic lavas	Recharge area	Springs	3	2623	0.4 - 0.8	0.6	194
Lemurge DAD	Flow-through area	Springs	16	2136	1.7 - 61.7	23.0	409
	Discharge area	Springs	6	1838	12.8 - 42.5	24.8	446

3.4.4. Western flank

On the western flank of Mount Meru, in Mamsa, all water samples are from the flow-through areas, one sample (spring water) is from the nephelinite lavas and breccias covered with mantling ash at an intermediate elevation while six samples (well waters) are from the confined aquifer composed of weathered fractured lava at the base of the Mount Meru, overlaid by the alluvial fan deposits. The alluvial fan deposits are recent and found in shallow depth, hence the groundwater mineralisation in the wells is mainly influenced by the weathered fractured lava deposit. Table 7 shows that there is a significant progressive mineralisation of the groundwater along the flow path (increase in TDS) but with similar F^- values, this suggests that the weathered fractured lava contains less F^--rich minerals. On the western flank, F^- remains relatively limited (3.4–3.7 mg/L), at least below Tanzanian limit. This suggests that the western flank groundwater could be a better opportunity for Arusha water-supply, compared to the sources they are using now.

Table 7. Descriptive statistics of F^- and TDS values in the water samples from different geological formations and different flow system zones on the western flank of Mount Meru.

Geological formation	Zone	Water source	n	Average elevation (m)	Average well depth (m)	F^- (mg/l)		Average TDS (mg/l)
						Range	Mean	
Nephelinite lavas and breccias covered with Mantling ash	Flow-through area	Spring	1	2240			3.4	590
Weathered fractured lava covered with alluvial fan deposits	Flow-through area	Shallow wells	6	1649	44	3.4 - 4.0	3.7	1017

3.4.5. South-western flank

Table 8 shows that the springs that are located in the mantling ash in the upper part of the flow-through area show low mineralisation but with high F^- values compared to the springs and shallow wells in the middle part of the flow-through area located in the pyroclastics with subordinate nephelinitic and phonolitic lavas covered with mantling ash. This indicates their low mineralisation is due to short water residence times, as they are located just near the

boundary between the mantling ash and the pyroclastics with subordinate nephelinitic and phonolitic lavas where the groundwater recharge occurs at higher elevations. Their higher F^- values are influenced by the mantling ash deposits which can readily release a high amount of F^- (Ghiglieri et al., 2012). The mantling ash deposits are very loose and fine-grained; therefore, they are highly weatherable and readily dissolve in water compared to the lava deposits. Water samples from the shallow wells located in the alluvial deposits show a slight increase in mineralisation with comparable F^- values compared to the samples from the mantling ash deposits in the middle part of the flow-through area; this suggests that the progressive mineralisation occurring in the shallow depths of the alluvial deposits is not accompanied by a considerable increase in F^-. The water samples from the deep wells located in the alluvial deposits in the lower part of the flow-through area show low mineralisation but with comparable F^- values as the samples from the pyroclastics with subordinate nephelinitic and phonolitic lavas covered with mantling ash located in the middle part of the flow-through area. These are deep circulating waters which have undergone deep infiltration in the recharge area at higher elevations (see Fig. 5). The alluvial deposits are found at the base of Mount Meru. These deposits are recent and found in shallow depth. Here the F^- values of deep circulating waters are mainly influenced by the weathered fractured lava which is composing the deep aquifer (Bennett et al., 2021). Thus, the low mineralisation in the deep circulating waters is attributed to slow weathering and dissolution of aluminosilicate minerals in the weathered fractured lava (Bennett et al., 2021). Furthermore, the samples from the shallow wells located in the alluvium deposits in the lowest part of the flow-through area show significant mineralisation but lower F^- values compared to the rest of the samples in the entire flow zone. These are mixture of deep circulating waters and shallow flow waters (see Fig. 5). On the south-western flank, the shallow wells in the flow-through area on alluvium deposits provide groundwater with relatively low F^- below Tanzanian limit (average 2.3 mg/L), whereas one of the three investigated deep wells in the flow-through area shows F^- below Tanzanian limit (3.8 mg/L), this suggests a possibility of finding more localities of lower F^- groundwater in the deep aquifer.

Table 8. Descriptive statistics of F^- and TDS values in the water samples from different geological formations and different flow system zones on the south-western flank of Mount Meru.

Geological formation	Zone	Water source	n	Average elevation (m)	Average well depth (m)	F^- (mg/l)		Average TDS (mg/l)
						Range	Mean	
Mantling ash	Flow-through area	Springs	2	1921		11.7 - 12.4	12.0	386
Pyroclastics with subordinate nephelinitic and phonolitic lavas covered with mantling ash	Flow-through area	Springs	6	1574		4.7 - 6.9	5.5	855
		Shallow wells	6	1572	11	2.9 - 12.0	6.0	763
Mantling ash	Flow-through area	Springs	4	1550		8.2 - 18.9	11.9	1246
		Shallow wells	33	1549	19	5.1 - 122	17.9	1161
Alluvial fan deposits	Flow-through area	Shallow wells	15	1543	25	4.5 - 60.4	13.3	1327
		Deep wells	3	1467	151	3.8 - 7.8	5.4	653
Alluvium	Flow-through area	Shallow wells	2	1379	6	2.0 - 2.5	2.3	893

603

604 Fig. 16 shows the identified low F^- zones on the flanks of Mount Meru, that could be used in
605 a healthy way (or suitable for blending, if only very small exceedance). From the discussion
606 above, high F^- values are found in the debris avalanche deposits, mantling ash, alluvial fan
607 deposits and lake deposits, whereas low F^- values are found in the pyroclastics and lavas. The
608 lavas deposits are more compact and less weatherable as compared to the DADs, mantling ash
609 and lake deposits. The DADs are brecciated with fine matrix while ash deposits are very loose
610 and fine-grained, these characteristics make them highly weatherable compared to lavas
611 deposits. Moreover, the lava deposits are found in higher elevations at the centre of Mount
612 Meru where there are steep slopes and lower temperatures. Steep slopes at this area lead to
613 shorter water residence time while lower temperatures hinder the enrichment of fluoride due to
614 low dissolution of fluoride-rich minerals. The DADs and ash deposits are found in lower
615 elevations at the base of the Mount Meru. At lower elevations, the areas have gentle slopes and
616 high temperatures compared to higher elevations in the mountain. The gentle slope and large
617 distance from the recharge area (the center of Mount Meru) favour long water residence time
618 while high temperature favours the enrichment of fluoride due to high dissolution of fluoride-
619 rich minerals. Furthermore, the deep wells show low mineralisation and low F^- values
620 compared to shallow wells, this is attributed to slow weathering and dissolution of
621 aluminosilicate minerals in the weathered fractured lava. This is suggesting that the deep rocks
622 are less weathered. Therefore, the internal texture and grain size of the geological formations
623 (causing variable weatherability), the burial depth of these formations (deep rocks are less
624 weathered) and the water residence times (which corresponds to the type of groundwater flow
625 system: local, intermediary or regional) determine the F^- concentrations in the groundwater in
626 relation to the geological formations.

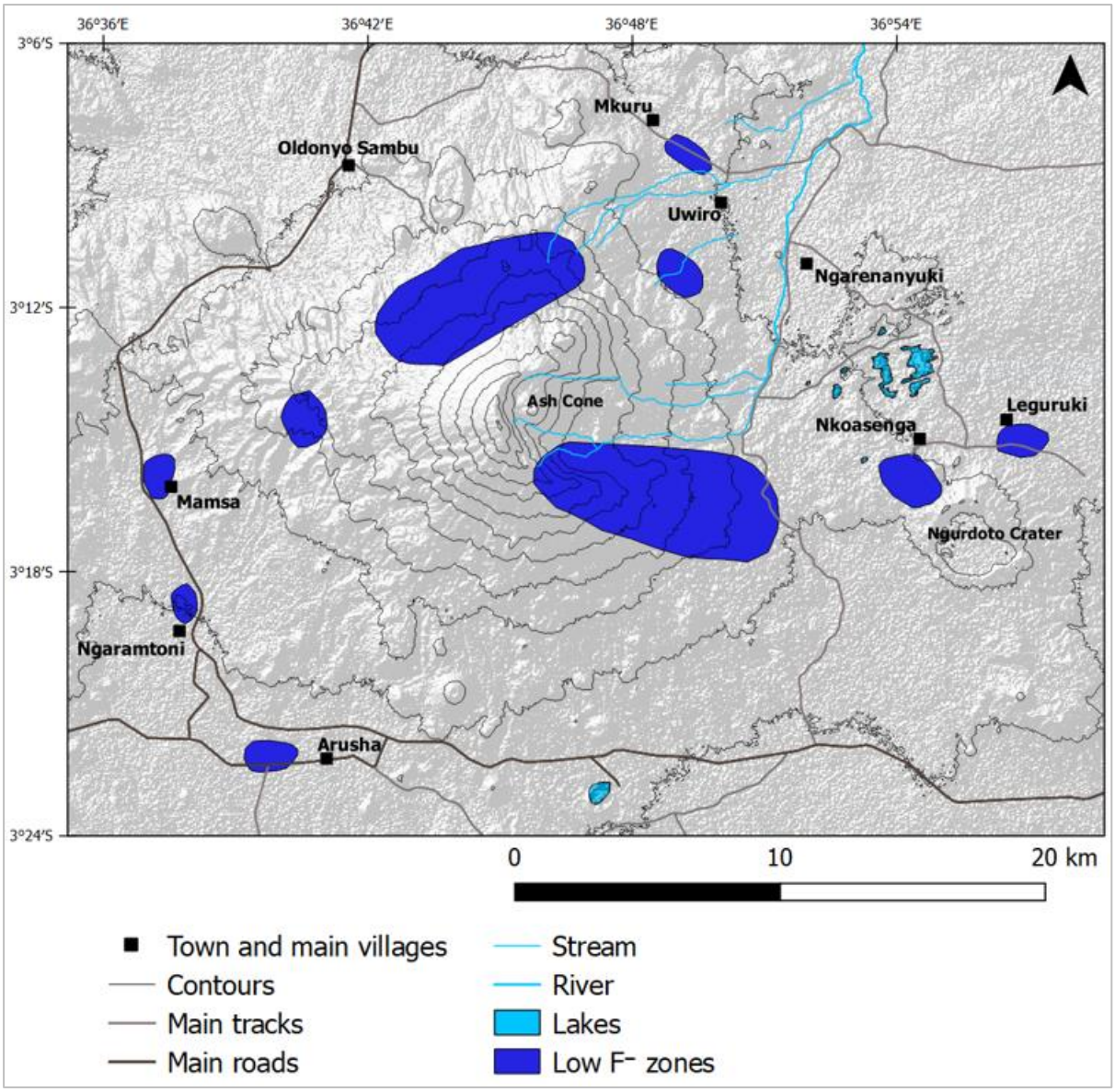

627

628 **Fig. 16.** A map showing the identified low F^- zones on the flanks of Mount Meru, Northern
629 Tanzania.

630 **4. Conclusions and recommendations**

631 The groundwater chemistry in the study area is controlled mainly by the dissolution of
632 weathering aluminosilicate minerals, dissolution of F^--bearing minerals, precipitation of
633 carbonate minerals and dissolution of volcanic gases. Evaporative concentration of solutes,
634 precipitation and redissolution of evaporitic salts may locally play a role, especially on the
635 north-eastern flank of Mount Meru. High F^- values are found in the debris avalanche deposits,
636 mantling ash, alluvial fan deposits and lake deposits, whereas low F^- values are found in the
637 pyroclastics and lavas deposits. The internal texture and grain size of geological formations
638 (causing variable weatherability), the burial depth of these formations (deep rocks are less

639 weathered) and the water residence times (corresponding to the groundwater flow system:
640 local, intermediary or regional) are the factors determining the F^- concentrations in the
641 groundwater in the area.
642 The low F^- groundwater sources which can be used for drinking water supply without health
643 impacts on the population under WHO limit (1.5 mg/L) are low-fluoride springs from the high-
644 altitude recharge areas on the eastern and north-western flanks of Mount Meru inside Arusha
645 National Park. The shallow aquifer on the western flank shows low F^- values that meet the
646 Tanzanian limit (4.0 mg/L). On the south-western flank, the alluvium deposits at lower
647 elevations contain water with low F^- which meet the Tanzanian limit, whereas the deep aquifer
648 shows a possibility of finding more localities of lower F^- groundwater as one of the three
649 investigated deep boreholes meets the Tanzanian limit.
650
651

Appendix

Table 9. Table. Major and minor physicochemical parameters of water samples. (units are in mg/L, except for the pH (unitless) and EC (µS/cm at 25°C). * as mg/L HCO_3^-).

Water source	Water point ID	Lab ID	pH	EC(µS/cm at 25°C)	Na^+	K^+	Ca^{2+}	Mg^{2+}	Fe^{2+}/Fe^{3+}	Mn^{2+}	NH_4^+	F^-	Cl^-	SO_4^{2-}	NO_3^-	NO_2^-	$(HCO_3^- + CO_3^{2-})$*	PO_4^{3-}	SiO_2	TDS
Eastern flank																				
Springs	S35	19/023	7.9	229	33.2	12.2	6.6	0.4	0.05	0.000	0.000	2.1	1.9	0.5	1.5	0.000	115	0.06	36.3	210
	S36	19/024	7.7	202	28.1	14.5	7.0	0.4	0.09	0.000	0.000	0.4	3.9	0.1	1.4	0.000	112	0.56	61.1	230
	S37	19/025	7.8	415	66.5	25.5	9.8	0.3	0.06	0.000	0.000	14.9	9.4	3.7	1.5	0.000	180	0.70	38.3	351
	S38	19/026	7.7	169	28.7	5.8	6.1	0.2	0.10	0.000	0.000	3.9	5.1	0.1	2.9	0.000	78.8	0.49	42.5	175
	S39	19/027	7.2	150	24.9	3.5	5.6	0.2	0.12	0.000	0.000	1.5	6.1	0.4	2.2	0.000	71.1	0.25	38.6	154
	S40	19/028	7.3	150	24.9	4.2	5.6	0.2	0.14	0.000	0.000	0.8	5.0	0.3	1.1	0.000	79.4	0.00	40.2	162
	S41	19/029	7.5	302	31.7	25.8	11.9	0.7	0.06	0.000	0.000	1.3	8.8	1.6	2.3	0.000	142	0.79	35.9	263
	S44	19/034	8.6	1183	424.5	51.3	1.6	0.5	0.03	0.007	0.006	274	18.8	67.5	1.7	0.002	317	0.70	27.2	1184
	S45	19/035	8.2	1123	402.4	58.1	1.4	0.4	0.03	0.007	0.007	254	16.7	68.3	2.4	0.011	330	0.79	28.7	1163
	S46	19/037	7.8	193	27.3	10.9	2.6	0.4	0.05	0.006	0.005	0.2	4.4	0.1	1.1	0.003	96	0.02	46.8	190
	S47	19/039	7.4	232	27.8	20.5	4.1	0.5	0.04	0.005	0.010	0.6	5.5	0.0	5.4	0.002	112	0.05	36.3	213
	S47'	19/040	7.1	148	20.6	10.2	1.0	0.2	0.05	0.004	0.006	0.4	4.5	0.0	2.2	0.003	67.8	0.06	38.7	146
	S47''	19/041	7.3	105	15.1	4.9	1.3	0.2	0.04	0.002	0.001	0.1	4.2	0.0	4.0	0.002	44.5	0.03	42.4	117
	STP7	19/006	7.9	270	64.1	7.4	7.5	0.9	0.04	0.000	0.000	21.4	1.7	3.5	0.0	0.000	121	0.64	35.7	264
	STP8	19/007	7.9	312	34.9	35.4	10.6	0.7	0.05	0.000	0.000	1.5	5.8	1.2	3.9	0.000	179	0.02	36.8	310
	STP11	19/010	7.7	246	27.0	23.6	10.0	0.7	0.07	0.000	0.000	1.0	3.9	0.4	3.3	0.000	141	0.00	35.2	246
Hydrothermal springs	S42	19/030	8.2	3650	899	179	8.4	1.6	0.07	0.000	0.000	301	100	260	2.5	0.004	1287	0.00	31.4	3070
	S43	19/032	8.5	4590	1123	216	3.8	2.3	0.04	0.006	0.016	95.2	148	418	0.9	0.000	2170	0.96	36.3	4214
Stream	STP9	19/008	9.1	4390	1140	220	9.1	2.2	0.06	0.000	0.000	553	295	377	1.1	0.000	914	0.79	27.6	3540
Lakes	L1	19/001	9.5	8630	1928	283	5.7	2.7	0.12	0.001	0.000	217	192	517	6.0	0.003	4285	1.98	0.3	7438
	L2	19/002	9.9	19820	5190	801	7.6	3.8	0.18	0.001	0.000	1004	512	102	5.1	0.051	9862.7	6.52	0.9	17495
	L3	19/003	10.1	17570	4240	714	7.3	1.5	0.16	0.005	0.000	988	434	10.4	7.1	0.041	9284.5	1.97	2.2	15691
Far east of the eastern flank (Northern flank of Ngurdoto crater)																				
Springs	S1	18/120	7.2	632	106	26.2	14.0	2.4	0.02	0.008	0.075	2.6	13.4	19.8	10.0	0.002	334	0.05	44.5	573
	S2	18/119	7.6	919	171	42.8	2.4	0.4	0.02	0.012	0.038	10.7	3.3	25.7	23.5	0.078	478	0.60	30.8	789
Shallow wells	W1	18/121	7.1	740	115	36.3	8.4	2.3	0.06	0.002	0.043	4.6	10.6	9.3	5.3	0.003	378	0.13	44.1	614
	W2	18/122	7.2	823	126	30.4	9.4	1.7	0.01	0.005	0.041	3.5	12.7	42.6	50.3	1.292	319	0.49	41.5	639
	W3	19/307	7.2	722	132	34.8	13.1	2.9	0.05	0.003	0.010	3.5	6.6	21.9	19.4	1.137	404	1.16	54.3	695
	W4	19/060	8.3	882	185	33.9	6.5	1.3	22.32	0.300	0.040	41.5	10.6	34.7	31.8	0.000	343	0.76	149	861
	W5	19/061	8.3	1932	443	60.1	3.1	1.3	0.00	0.150	0.000	134	14.6	68.7	101.1	0.000	756	0.31	62.3	1644
	W8	18/123	7.4	943	152	25.6	15.4	1.3	0.01	0.000	0.067	8.2	26.3	42.9	65.1	0.005	349	0.12	38.4	724
	W9	19/062	8.4	487	65	23.7	10.5	2.9	20.46	0.210	0.000	1.0	3.6	9.1	0.7	0.000	255	0.56	147	539
	W10	19/308	7.3	798	117	51.1	22.8	7.1	0.05	0.005	0.002	4.5	5.5	37.6	12.2	0.001	435	0.64	40.3	734
	W13	19/063	8.3	487	58	17.7	3.0	0.4	11.05	0.060	0.000	1.3	8.2	21.1	3.4	0.000	186	1.17	195	506
	W14	19/064	8.2	515	75	28.8	17.0	4.0	1.01	0.090	0.000	1.6	9.1	13.3	0.0	0.000	296	0.00	194	640
	W16	19/065	8.1	548	70	20.9	28.9	3.7	0.00	0.000	0.000	2.8	7.5	18.6	0.6	0.000	255	0.00	179	587
	W18	19/066	7.6	515	82	23.7	7.2	1.8	2.88	0.150	0.000	7.4	12.0	31.2	2.3	0.000	227	0.56	154	552
	W19	19/067	8.1	849	126	58.5	3.9	1.0	36.44	0.090	0.000	30.7	7.4	3.4	0.0	0.000	425	0.35	157	850
Water pond	WP	19/314	9.2	4310	789	268.5	25.7	5.7	0.2	0.019	0.045	85.9	62.1	254	5.9	0.126	1730	8.19	1.9	3237

656 **Table 9**. Continued

Water source	Water point ID	Lab ID	pH	EC(µS/cm at 25°C)	Na^+	K^+	Ca^{2+}	Mg^{2+}	Fe^{2+}/Fe^{3+}	Mn^{2+}	NH_4^+	F^-	Cl^-	SO_4^{2-}	NO_3^-	NO_2^-	$(HCO_3^- + CO_3^{2-})$*	PO_4^{3-}	SiO_2	TDS
North-eastern flank																				
	S6	17/097	7.7	1736	401	49.4	10.4	2.5	0.06	0.004	0.011	35.0	24.8	119	29.0	0.004	832	0.00	54.0	1556
	S6	19/092	8.4	2060	509	63.6	13.0	2.8	0.50	0.140	0.000	74.6	30.1	155	56.0	0.000	906	0.28	176	1987
	S7	17/098	7.8	1742	377	46.2	10.5	2.5	0.07	0.006	0.006	37.3	24.9	111	27.9	0.181	844	0.00	58.4	1540
	S7	19/093	8.5	2120	517	69.4	14.1	2.9	0.40	0.230	0.060	78.2	31.3	173	59.1	0.000	1039	0.28	208	2193
	S11	17/099	7.2	1189	221	44.1	28.1	8.3	0.01	0.003	0.098	5.8	14.8	42.4	3.2	0.014	627	0.00	56.6	1051
	S11	18/135	7.2	1219	201	35.9	36.0	8.2	0.03	0.003	0.167	3.0	5.5	41.9	6.1	0.000	716	0.61	51.6	1105
	S11	19/011	8.5	1205	231	54.2	13.3	7.2	0.05	0.000	0.000	4.2	13.2	18.2	2.1	0.002	764	0.67	57.4	1166
	S12	17/100	7.0	873	162	32.3	18.9	11.2	0.12	0.003	0.142	5.5	13.0	38.1	7.0	0.015	461	0.00	58.1	807
	S12	19/094	8.4	888	126	47.8	22.4	7.2	0.21	0.030	0.000	6.3	15.7	49.1	14.8	0.000	423	0.84	210	923
	S13	17/101	7.3	786	171	27.7	9.8	3.3	0.05	0.003	0.000	8.8	15.0	31.4	5.3	3.731	400	0.00	51.0	727
	S13	18/124	7.5	802	132	20.8	9.3	2.5	0.00	0.000	0.149	6.2	8.0	21.2	6.9	0.000	394	1.00	47.0	649
	S13	19/012	7.8	790	141	32.2	14.1	2.3	0.06	0.000	0.000	9.6	13.4	18.7	4.5	0.000	420	1.21	54.6	712
	S14	17/102	7.5	906	199	34.0	11.3	3.5	0.08	0.004	0.000	9.7	18.4	38.1	3.3	0.636	466	0.00	48.2	832
Springs	S14	19/095	8.4	977	218	51.4	11.1	3.8	0.24	0.400	0.000	15.8	22.4	36.6	3.4	0.000	515	1.05	167	1047
	S15	17/103	7.4	1065	224	41.2	17.2	4.5	0.06	0.003	0.105	9.8	17.3	58.3	20.1	0.006	533	0.00	46.1	972
	S15	18/125	7.4	1144	180	34.1	19.5	4.4	0.01	0.003	0.108	7.2	11.2	49.6	25.2	0.865	535	0.64	44.9	913
	S15	19/013	7.7	1134	201	53.4	18.3	4.3	0.06	0.000	0.000	12.5	17.1	70.2	28.9	0.330	561	1.00	38.9	1007
	S18	17/106	8.0	3500	708	104	10.6	4.1	0.03	0.001	0.345	30.2	114	472	11.3	0.003	1335	0.00	25.6	2815
	S18	18/136	8.0	3510	762	90.5	12.2	3.4	0.01	0.004	0.144	24.9	136	379	14.6	0.000	1616	0.16	26.8	3066
	S18	19/017	8.2	3500	817	124	12.1	3.3	0.06	0.000	0.000	90.2	119	434	10.4	0.000	1316	0.21	27.3	2954
	S19	17/107	8.1	3490	712	105	10.8	3.9	0.01	0.005	0.303	41.2	113	425	8.8	0.021	1333	0.00	24.0	2777
	S19	18/137	8.2	3490	753	93.0	12.8	3.5	0.03	0.003	0.119	29.4	134	393	15.0	0.000	1565	0.13	26.3	3025
	S19	19/018	8.3	3460	796	109	13.2	3.3	0.06	0.000	0.000	106.1	120	428	11.6	0.000	1250	0.19	15.6	2853
	STP4	18/139	6.9	321	63.0	8.3	1.9	0.5	0.02	0.003	0.016	4.2	4.0	9.7	4.5	0.000	158	1.68	39.8	295
	STP5	18/138	6.9	292	58.7	8.1	1.3	0.4	0.06	0.001	0.027	4.3	2.3	4.9	4.6	0.320	151	1.49	39.0	276
	STP6	17/128	8.1	3370	720	88.2	10.6	3.5	0.00	0.007	0.003	36.5	85.7	499	17.1	1.421	1342	0.00	16.9	2820
	STP6	19/105	8.6	3270	1012	119.5	8.8	3.6	0.00	0.150	0.000	113	80.7	448	28.1	0.000	1643	0.37	104	3560
	W11	17/108	7.6	1116	254	28.8	8.6	2.0	0.07	0.006	0.037	17.5	27.1	48.2	4.4	0.009	558	0.00	39.1	987
	W12	17/109	7.6	917	202	24.5	11.7	2.5	0.11	0.006	0.026	15.3	21.5	26.7	4.3	0.008	475	0.00	31.6	816
	W24	17/110	7.9	872	198	22.1	4.2	1.3	0.03	0.004	0.008	13.6	21.0	25.1	4.7	0.633	442	0.00	38.1	770
	W24	19/068	8.3	1182	287	33.5	4.0	0.8	2.84	2.480	0.050	30.1	52.9	59.7	18.1	0.000	540	1.36	154	1186
	W25	19/069	8.5	2680	579	80.9	8.3	6.4	2.25	0.240	0.080	121	78.3	204	12.7	0.000	1080	0.24	149	2322
Shallow wells	W70	17/124	7.7	973	215	18.5	6.2	1.3	2.14	0.018	0.012	11.7	23.2	38.3	5.1	0.054	483	0.00	50.7	854
	W71	17/125	7.8	875	185	16.3	5.1	1.0	0.10	0.008	0.000	13.6	20.6	28.4	3.6	0.007	431	0.00	24.2	729
	W71	19/083	8.4	905	215	32.7	3.6	0.3	30.8	1.260	0.030	27.2	22.5	11.0	0.0	0.000	518	0.46	124	986
	W91	19/087	8.3	846	192	25.6	4.9	0.9	19.49	2.010	0.030	19.2	22.1	27.5	1.6	0.000	488	0.55	80.2	884
	W95	19/088	8.3	741	148	29.4	2.7	0.3	1.08	0.100	0.000	9.1	18.9	20.3	3.2	0.000	362	0.40	160	755
	W96	19/089	8.3	874	207	27.0	9.4	2.2	4.38	0.380	0.060	14.1	20.5	22.7	4.3	0.000	492	0.12	136	940
	BH26	19/358	7.7	424	80.4	12.4	6.3	1.0	0.02	0.000	0.000	3.6	3.8	1.9	36.5	0.010	220	0.29	45.0	412
River	STP10	19/009	8.8	1736	464	87.2	9.3	1.2	0.08	0.000	0.000	144	45.1	126	1.1	0.002	645	0.55	20.8	1544

657

658 **Table 9**. Continued

Water source	Water point ID	Lab ID	pH	EC(µS/cm at 25°C)	Na^+	K^+	Ca^{2+}	Mg^{2+}	Fe^{2+}/Fe^{3+}	Mn^{2+}	NH_4^+	F^-	Cl^-	SO_4^{2-}	NO_3^-	NO_2^-	$(HCO_3^- + CO_3^{2-})$*	PO_4^{3-}	SiO_2	TDS
North-western flank																				
	S3	17/094	7.0	453	95.2	21.0	1.5	1.2	0.10	0.004	0.001	25.0	4.5	9.1	5.9	0.182	210	0.00	46.8	420
	S3	18/134	7.2	443	100.5	19.1	1.6	0.2	0.06	0.001	0.049	16.8	4.5	7.3	1.8	0.000	207	0.12	41.4	400
	S3	19/004	7.6	450	134.8	7.2	5.1	0.4	0.05	0.000	0.000	61.7	4.2	11.5	2.5	0.002	142	0.42	43.3	414
	S3	19/304	7.8	415	63.0	17.7	6.2	1.7	0.05	0.003	0.000	18.6	1.2	11.1	2.1	0.002	161	0.36	46.4	329
	S3	19/353	7.8	443	83.5	16.9	1.3	0.3	0.04	0.000	0.000	20.3	3.2	3.6	0.1	0.003	198	0.43	45.9	374
	S3'	19/090	8.2	438	105	23.8	1.3	0.3	0.66	0.000	0.040	49.1	6.4	11.2	0.0	0.000	146	0.24	142.7	487
	S4	17/095	7.8	439	84.7	21.4	1.7	1.1	0.02	0.006	0.000	18.1	4.1	12.9	16.2	2.438	189	0.00	44.0	396
	S4	19/091	8.1	430	90	29.4	1.4	0.2	0.54	0.000	0.050	29.9	6.9	9.0	19.0	0.000	134	0.36	154.5	475
	S4	19/354	7.3	435	78.75	20.4	1.2	0.2	0.03	0.000	0.000	14.9	2.9	2.7	12.4	0.004	196	0.38	42.1	372
	S5	17/096	7.3	445	80.7	22.6	1.8	1.0	0.04	0.004	0.921	17.8	4.2	13.2	10.5	1.762	188	0.00	43.0	386
	S5	18/133	7.2	437	97.9	15.4	1.6	0.2	0.17	0.005	0.052	10.7	4.6	7.9	16.1	0.508	198	0.14	38.7	392
	S5	19/005	7.4	441	103.6	24.3	5.4	0.3	0.04	0.000	0.000	35.0	3.9	9.7	13.3	0.001	168	0.37	42.5	406
Springs	S5	19/305	7.5	407	55.8	21.1	6.1	1.6	0.04	0.004	0.030	13.7	0.8	9.0	11.3	0.012	154	0.39	41.8	316
	S5	19/355	7.3	436	79.65	20.3	1.3	0.2	0.03	0.000	0.000	15.0	3.0	3.3	13.4	0.002	195	0.41	40.9	373
	S16	17/104	7.0	528	103.2	26.4	2.4	1.1	0.10	0.005	0.024	24.4	4.5	16.3	13.5	0.104	231	0.00	41.6	464
	S16	18/141	7.1	512	86	26.0	2.0	0.2	0.14	0.008	0.075	15.2	5.4	11.9	0.2	0.000	228	0.02	47.3	423
	S16	19/014	7.5	497	120.2	24.9	4.3	0.3	0.13	0.000	0.000	42.5	1.5	3.6	0.6	0.001	256	0.12	38.0	492
	S16'	18/140	7.0	487	84.8	24.7	3.1	0.3	0.02	0.002	0.051	12.8	6.2	13.4	5.0	0.000	224	0.00	38.9	413
	S16'	19/015	7.6	480	112.9	25.3	5.0	0.4	0.05	0.000	0.000	36.3	3.2	5.3	1.9	0.000	248	0.42	40.9	480
	S16'	19/356	6.7	472	87.6	20.7	2.2	0.4	0.14	0.002	0.004	17.6	3.7	1.9	10.1	0.026	220	0.06	41.7	406
	S48	19/042	7.2	205	28.6	8.3	3.7	1.2	0.20	0.001	0.004	0.4	5.9	0.2	0.9	0.004	101	0.00	34.3	185
	S_TP1	19/101	8.3	152	17.0	8.6	2.2	0.3	2.69	0.050	0.000	0.5	3.4	0.4	0.5	0.000	59.0	0.00	96.7	191
	S_TP2	19/102	8.1	547	120	13.2	5.8	0.8	0.00	0.000	0.030	19.4	7.5	11.1	0.7	0.000	292	0.53	146.1	617
	S_TP3	19/103	8.1	323	65	17.2	2.8	0.6	8.03	0.000	0.000	1.7	5.1	0.2	0.0	0.000	205	0.10	78.1	384
	S_TP4	19/104	8.2	175	18.0	9.9	4.4	0.4	2.93	0.000	0.000	0.8	4.1	0.3	2.0	0.000	78	0.00	86.4	207
Western flank																				
Spring	S49	19/043	8.4	719	111	23.4	16.4	3.1	0.03	0.000	0.015	3.4	7.7	14.0	6.0	0.004	365	0.17	40.1	590
	W28	19/070	8.5	1022	186	38.2	30.9	4.8	2.96	0.090	0.090	4.0	26.6	72.4	44.3	0.000	525	0.07	170.5	1106
	W29	17/111	7.5	1204	185	38.1	55.4	11.5	0.00	0.004	0.071	3.9	27.9	60.0	41.3	16.46	522	0.00	44.7	1006
Shallow wells	W29	18/126	7.4	1185	177	33.4	51.5	5.5	0.01	0.002	0.103	3.6	23.7	91.7	34.3	0.000	562	0.14	44.9	1028
	W29	19/020	7.8	1174	185	46.8	25.9	5.3	0.06	0.000	0.000	3.4	27.2	84.5	33.4	0.000	530	0.05	50.7	992
	W30	18/127	7.6	1171	161	29.7	48.6	5.1	0.12	0.000	0.096	3.4	21.4	76.3	35.5	0.002	527	0.03	43.6	952
	W30	19/021	8.0	1153	187	53.5	26.1	4.7	0.06	0.000	0.000	3.7	27.5	65.9	31.2	0.000	567	0.10	49.2	1016

659

660 **Table 9**. Continued

Water source	Water point ID	Lab ID	pH	EC(µS/cm at 25°C)	Na^+	K^+	Ca^{2+}	Mg^{2+}	Fe^{2+}/Fe^{3+}	Mn^{2+}	NH_4^+	F^-	Cl^-	SO_4^{2-}	NO_3^-	NO_2^-	$(HCO_3^- + CO_3^{2-})$*	PO_4^{3-}	SiO_2	TDS
South-western flank																				
Springs	S17	17/105	7.2	1393	245	121	25.1	3.5	0.00	0.003	0.040	11.8	13.4	53.4	10.6	1.624	743	0	49.3	1278
	S17	18/130	7.4	1464	233	49.6	38.6	4.4	0.02	0.003	0.101	8.2	25.3	14.1	29.7	0.007	790	0.08	45.1	1238
	S17	19/016	7.7	1447	310	61.9	11.7	2.9	0.06	0.000	0.000	18.9	20.8	3.9	29.9	0.000	873	0.22	47.9	1381
	S20	19/096	8.3	765	144	45.0	14.7	3.6	0.52	0.080	0.000	6.9	13.2	22.8	44.6	0.000	380	0.00	191	867
	S21	19/097	8.3	771	145	47.4	15.5	4.2	0.09	1.310	0.070	5.8	13.0	22.8	37.6	0.000	387	0.06	200	880
	S22	19/098	8.3	863	168	54.4	24.4	7.9	0.00	0.030	0.040	5.2	18.1	30.1	58.9	0.000	476	0.04	197	1040
	S22	19/306	7.1	781	115	52.6	22.7	6.1	0.04	0.003	0.157	4.7	12.4	25.7	37.4	0.008	398	0.13	54.1	728
	S22	19/357	7.4	822	119	45.8	20.6	3.9	0.02	0.000	0.000	5.5	13.4	13.9	0.0	0.002	405	0.11	33.0	660
	S24	19/099	8.3	819	147	56.5	26.7	8.6	0.09	0.000	0.120	5.2	15.9	29.7	64.2	0.000	412	0.07	191	957
	S25	19/100	8.3	1010	195	65.5	17.3	4.0	0.69	0.140	0.060	8.8	20.6	17.5	57.2	0.000	527	0.20	175	1089
	S50	19/044	7.7	465	77.0	20.4	4.2	0.7	0.03	0.006	0.005	11.7	5.5	6.9	2.2	0.003	216	0.15	38.2	383
	S51	19/045	8.2	464	75.8	25.2	4.5	0.7	0.03	0.005	0.003	12.4	6.7	8.1	3.9	0.030	209	0.25	42.8	389
Shallow wells	W31	17/112	7.4	1370	285	50.2	12.7	5.6	0.03	0.004	0.039	9.8	21.0	43.0	40.7	6.124	668	0.00	44.4	1186
	W31	19/071	8.4	1452	271	59.9	22.9	5.5	0.53	0.210	0.140	13.6	28.5	31.3	80.7	0.000	675	0.04	168	1357
	W32	18/129	7.3	1451	244	44.8	33.3	4.2	0.02	0.000	0.077	10.1	22.6	17.9	34.2	0.154	786	0.13	46.2	1243
	W32	19/022	7.7	1429	240	61.0	13.6	3.7	0.06	0.000	0.000	17.8	17.5	51.4	26.5	0.000	681	0.13	30.4	1142
	W33	19/072	8.4	1246	220	73.2	18.6	5.1	0.12	0.130	0.000	8.5	31.1	59.4	75.5	0.000	610	0.03	175	1276
	W36	19/073	8.4	1729	305	90.2	16.6	3.9	0.00	0.000	0.000	13.5	28.7	59.2	129.2	0.000	680	0.11	159	1485
	W39	19/074	8.5	1379	228	60.8	38.4	6.5	0.57	0.130	0.100	9.3	22.1	49.1	59.2	0.000	620	0.24	162	1257
	W40	19/075	8.5	1557	272	68.0	48.0	8.1	0.00	0.000	0.050	6.8	26.2	76.1	79.8	0.000	708	0.23	178	1471
	W42	19/031	7.7	1680	346	65.0	27.6	4.4	0.02	0.007	0.017	8.1	26.5	62.3	43.8	0.005	949	0.27	50.5	1583
	W43	19/033	8.0	1733	330	52.3	24.4	3.5	0.03	0.006	0.012	22.4	33.2	46.8	84.0	0.006	875	0.89	51.2	1524
	W44	17/113	7.7	1711	366	43.2	25.7	5.0	0.00	0.003	0.039	11.4	21.7	52.7	21.0	2.530	898	0.00	44.9	1491
	W45	19/036	8.1	1290	271	36.3	5.3	1.5	0.03	0.001	0.006	60.4	11.6	19.1	27.6	0.004	602	1.05	50.0	1086
	W46	17/114	7.3	729	162	29.8	9.3	1.8	0.00	0.005	0.019	6.2	6.8	22.1	20.9	0.450	400	0.00	38.6	697
	W46	18/132	7.1	870	150	26.5	11.9	1.3	0.01	0.005	0.050	5.1	10.0	23.6	19.4	0.000	443	0.20	39.3	731
	W46	19/038	7.6	900	168	36.3	9.4	1.2	0.03	0.005	0.007	7.7	10.2	27.8	22.0	0.005	476	0.31	45.9	805
	W48	17/115	7.5	1689	379	47.1	14.1	2.8	0.01	0.005	0.000	16.4	11.7	16.4	20.0	2.285	999	0.00	47.8	1557
	W48	19/076	8.5	1672	387	81.7	10.8	2.2	1.25	0.220	0.120	44.8	14.1	9.7	19.0	0.000	910	0.54	187	1669
	W49	17/116	7.8	1562	336	38.2	15.5	2.6	0.00	0.007	0.283	25.6	6.3	12.6	13.1	1.603	917	0.00	42.9	1412
	W51	17/117	7.8	1738	367	42.5	17.3	2.5	0.00	0.007	0.000	33.3	13.3	24.2	27.0	2.562	877	0.00	46.1	1452
	W51	19/077	8.5	1773	425	57.7	12.8	2.3	0.00	0.060	0.000	122	14.7	8.7	50.8	0.000	890	1.66	180	1766
	W52	19/019	7.8	1552	378	54.0	12.5	5.3	0.07	0.000	0.000	6.3	27.7	48.7	6.5	0.000	939	0.25	45.2	1524
	W55	17/118	7.2	945	165	47.9	13.8	3.8	0.00	0.004	0.363	7.9	9.4	24.0	9.0	0.337	465	0.00	46.9	794
	W55	19/078	8.5	984	163	64.3	12.6	4.7	0.23	0.020	0.000	11.2	14.2	27.7	22.0	0.000	466	0.05	192	978
	W57	17/119	7.2	1012	172	49.0	14.5	4.4	0.00	0.003	0.010	6.6	12.0	29.3	11.5	3.138	501	0.00	46.0	849
	W57	19/079	8.4	1038	176	71.3	12.9	4.6	0.18	0.190	0.000	9.5	16.5	10.5	29.3	0.000	505	0.23	176	1012
	W58	19/046	7.5	974	167	63.7	7.6	2.8	0.03	0.001	0.011	14.1	8.0	16.3	6.0	0.003	537	0.10	54.3	876
	W60	17/120	7.3	972	194	51.5	11.7	2.3	0.00	0.005	1.309	7.6	8.6	22.3	9.1	3.518	542	0.00	41.2	894
	W60	19/080	8.4	1007	173	89.6	10.6	2.6	0.00	0.040	0.040	13.7	12.1	25.3	35.8	0.000	473	0.04	171	1007
	W62	19/047	7.5	850	144	43.3	10.3	2.3	0.03	0.003	0.008	12.8	12.1	22.4	28.0	0.002	414	0.20	45.1	734
	W63	17/121	7.2	722	121	29.1	17.7	5.4	0.00	0.005	0.009	5.5	6.3	18.2	10.6	0.017	355	0.00	42.1	610

661 **Table 9**. Continued

Water source	Water point ID	Lab ID	pH	EC(µS/cm at 25°C)	Na^+	K^+	Ca^{2+}	Mg^{2+}	Fe^{2+}/Fe^{3+}	Mn^{2+}	NH_4^+	F^-	Cl^-	SO_4^{2-}	NO_3^-	NO_2^-	$(HCO_3^- + CO_3^{2-})$*	PO_4^{3-}	SiO_2	TDS
South-western flank continued																				
	W63	19/081	8.4	728	137	41.0	14.2	5.2	0.00	0.000	0.150	6.8	12.4	16.8	48.3	0.000	355	0.18	179	816
	W64	17/122	8.1	1543	324	48.8	7.9	6.4	0.00	0.018	0.017	6.4	23.4	46.7	46.1	0.415	809	0.00	38.9	1358
	W64	19/082	8.3	1382	280	54.5	45.7	7.8	0.59	0.040	0.000	7.3	25.4	53.8	69.0	0.000	735	0.20	164	1443
	W65	19/048	7.8	1658	317	57.3	29.5	4.1	0.03	0.011	0.011	9.7	20.9	56.4	45.9	0.005	906	0.25	52.8	1500
	W66	18/128	7.7	1402	262	28.1	23.2	3.0	0.01	0.000	0.086	8.9	16.6	15.7	8.9	0.004	814	0.91	40.7	1222
	W66	19/049	8.0	1420	285	44.7	20.3	3.0	0.03	0.006	0.007	21.7	15.1	30.8	6.8	0.002	820	1.05	48.8	1298
	W68	17/123	7.5	1411	254	44.6	42.1	6.0	0.00	0.006	0.018	4.9	20.5	55.6	28.6	3.016	687	0.00	40.1	1187
	W69	19/050	8.2	2320	415	79.8	12.5	2.6	0.04	0.000	0.009	17.0	67.0	88.7	258	0.010	857	0.83	19.0	1817
	W74	17/126	7.3	1005	202	27.1	14.1	1.8	0.00	0.006	0.000	8.9	10.1	33.9	20.1	5.420	541	0.00	45.0	909
	W74	19/084	8.3	961	195	32.2	9.1	1.1	0.22	0.050	0.000	13.9	11.7	11.9	27.9	0.000	536	0.16	193	1032
	W75	19/051	7.6	1045	173	69.1	14.0	3.5	0.03	0.008	0.011	9.7	16.1	34.0	21.6	0.003	534	0.03	48.1	923
	W76	19/052	7.6	1061	174	76.5	12.7	3.0	0.03	0.009	0.011	12.0	14.7	24.3	44.8	0.005	528	0.19	17.4	907
Shallow wells	W77	19/053	7.6	931	161	62.6	10.5	3.2	0.03	0.005	0.009	11.5	12.0	32.6	18.1	0.004	479	0.10	56.8	848
	W80	17/127	7.4	1281	223	51.0	7.4	5.6	0.00	0.006	1.161	5.3	20.4	44.8	19.3	1.209	640	0.00	40.0	1058
	W80	18/131	7.4	1277	207	51.4	38.1	5.2	0.40	0.000	0.102	4.5	24.6	24.3	21.4	0.000	729	0.05	46.6	1152
	W80	19/054	7.6	1294	208	71.6	27.4	4.2	0.03	0.003	0.013	6.4	21.1	41.3	19.6	0.006	705	0.07	36.3	1140
	W82	19/055	8.2	1432	288	44.6	23.1	2.8	0.04	0.008	0.012	10.4	21.8	46.1	15.5	0.003	793	0.83	43.6	1290
	W83	19/056	7.5	1200	192	74.9	17.4	3.6	0.02	0.001	0.009	7.4	26.5	47.7	68.4	0.003	551	0.11	37.4	1026
	W85	19/085	8.3	721	104	35.9	19.9	6.3	6.88	0.150	0.040	2.9	12.4	10.8	28.0	0.000	347	0.03	209	783
	W86	19/086	8.2	768	125	63.7	10.5	4.1	0.13	0.020	0.000	5.3	6.9	19.7	26.1	0.000	373	0.00	184	818
	W87	19/057	7.9	1713	348	59.0	18.7	2.7	0.02	0.002	0.010	41.1	16.1	23.9	16.4	0.002	978	1.05	2.4	1507
	W90	19/058	8.1	2050	392	99.0	8.9	2.4	0.03	0.005	0.012	45.1	16.3	38.8	10.2	0.008	1114	0.56	29.9	1757
	W92	19/309	7.1	980	164	61.9	19.9	5.1	0.06	0.006	0.003	6.3	12.2	36.2	32.7	0.023	510	0.15	47.9	896
	W93	19/059	8.0	715	112	34.6	16.0	3.2	0.44	0.001	0.020	3.4	10.8	13.0	3.1	0.014	404	0.25	42.5	643
	W100	19/310	8.2	1019	88.3	33.1	54.1	24.6	0.05	0.004	0.008	2.0	34.6	37.0	134	0.004	378	0.23	58.3	845
	W101	19/311	8.2	1116	130	40.6	68.0	16.9	0.05	0.004	0.004	2.5	47.2	57.6	167	1.330	356	0.40	53.6	941
Deep wells	BH3	19/313	8.0	726	121	33.4	25.5	6.9	0.05	0.006	0.071	3.8	7.9	19.5	7.2	0.001	433	0.54	51.9	710
	BH14	19/312	7.6	769	133	27.7	24.5	6.0	0.05	0.005	0.002	4.6	8.8	21.8	9.1	0.004	457	0.65	48.1	742
	BH28	19/359	7.5	606	105	21.9	7.9	1.6	0.03	0.000	0.000	7.8	5.7	7.3	0.0	0.054	310	0.53	40.4	508

662

663 **Acknowledgments**

664 The authors thank the Tanzania Commission for Science and Technology (COSTECH) and
665 Tanzania National Parks Authority (TANAPA) for providing research permits. Also, the
666 authors thank Laura Segers and Stefanie Rombaut for their assistance during fieldworks.
667 Thanks to Martine Leermakers and Natacha Brion (AMGC, Vrije Universiteit Brussel) for their
668 help with chemical analysis of some water samples. Ines Tomašek acknowledges the support
669 received from the VUB Strategic Research Program (SRP) and the Agence Nationale de la
670 Recherche of the French government through the program "Investissements d'Avenir" (16-

IDEX-0001 CAP 20-25). Karen Fontijn acknowledges support from F.R.S.-FNRS MIS grant F.4515.20. We also thank the two anonymous reviewers for their thoughtful comments that greatly improved this manuscript. Findings and conclusions in this paper are those of the authors and do not necessarily represent the official position of VLIR-UOS.

Funding

This research was funded by the Flemish Interuniversity Council - University Development Cooperation (VLIR-UOS) in the framework of project TZ2017TEA450A105 'Optimizing the valorization of water and rock resources for improved livelihoods in the Arusha volcanic region'.

References

American Public Health Association (APHA), American Water Works Association (AWWA), Water Environment Federation (WEF), 2017. Standard methods for the examination of water and wastewater, 23rd edition. American Public Health Association, Washington DC.

Bennett, G., Van Reybrouck, J., Shemsanga, C., Kisaka, M., Tomašek, I., Fontijn, K., Kervyn, M., Walraevens, K., 2021. Hydrochemical characterisation of high-fluoride groundwater and development of a conceptual groundwater flow model using a combined hydrogeological and hydrochemical approach on an active volcano: Mount Meru, Northern Tanzania. Water, 13 (16), 2159. doi: 10.3390/w13162159.

Chacha, N., Njau, K.N., Lugomela, G.V., Muzuka, A.N.N., 2018. Hydrogeochemical characteristics and spatial distribution of groundwater quality in Arusha well fields, Northern Tanzania. Applied Water Science, 8(4), 118. doi: 10.1007/s13201-018-0760-4.

Coetsiers, M., Kilonzo, F., Walraevens, K., 2008. Hydrochemistry and source of high fluoride in groundwater of the Nairobi area, Kenya / Hydrochimie et origine des fortes concentrations en fluorure dans l'eau souterraine de la région de Nairobi, au Kenya. Hydrological Sciences Journal, 53(6), 1230–1240. doi: 10.1623/hysj.53.6.1230.

Delcamp, A., Kervyn, M., Benbakkar, M., Kwelwa, S., Peter, D., 2017. Large volcanic landslide and debris avalanche deposit at Meru, Tanzania. Landslides, 14(3), 833–847. doi: 10.1007/s10346-016-0757-8.

Ghiglieri, G., Pittalis, D., Cerri, G., Oggiano, G., 2012. Hydrogeology and hydrogeochemistry of an alkaline volcanic area: the NE Mt. Meru slope (East African Rift – Northern Tanzania). Hydrology and Earth System Sciences, 16(2), 529–541. doi: 10.5194/hess-16-529-2012.

Hu, S., Luo, T., Jing, C., 2013. Principal component analysis of fluoride geochemistry of groundwater in Shanxi and Inner Mongolia, China. Journal of Geochemical Exploration, 135, 124–129. doi: 10.1016/j.gexplo.2012.08.013.

Ijumulana, J., Ligate, F., Bhattacharya, P., Mtalo, F., Zhang, C., 2020. Spatial analysis and GIS mapping of regional hotspots and potential health risk of fluoride concentrations in groundwater of northern Tanzania. Science of The Total Environment, 735, 139584. doi: 10.1016/j.scitotenv.2020.139584.

Ingebritsen, S.E., Geiger, S., Hurwitz, S., Driesner, T., 2010. Numerical simulation of magmatic hydrothermal systems. Review of Geophysics, 48(1), 1–33. doi: 10.1029/2009RG000287.

Jasim, A., Hemmings, B., Mayer, K., Scheu, B., 2018. Groundwater flow and volcanic unrest. In Gottsmann, J., Neuberg, J., Scheu, B. (Eds.), Volcanic unrest. Advances in volcanology. Springer, Cham. doi: 10.1007/11157_2018_33.

Kilham, P., Hecky, R.E., 1973. Fluoride: Geochemical and ecological significance in East African waters and sediments. Limnology and Oceanography, 18(6), 932–956. doi: 10.4319/lo.1973.18.6.0932.

Kitalika, A.J., Machunda, R.L., Komakech, H.C., Njau, K.N., 2018. Fluoride variations in rivers on the slopes of Mount Meru in Tanzania. Journal of Chemistry, 2018, 7140902. doi: 10.1155/2018/7140902.

Kumar, P., Singh, C.K., Saraswat, C., Mishra, B., Sharma, T., 2017. Evaluation of aqueous geochemistry of fluoride enriched groundwater: A case study of the Patan district, Gujarat, Western India. Water Science, 31(2), 215–229. doi: 10.1016/j.wsj.2017.05.002.

Luo, W., Gao, X., Zhang, X., 2018. Geochemical processes controlling the groundwater chemistry and fluoride contamination in the Yuncheng Basin, China – An area with complex hydrogeochemical conditions. PLoS ONE, 13(7), e0199082. doi: 10.1371/journal.pone.0199082.

Makoba, E., Muzuka, A.N.N., 2019. Water quality and hydrogeochemical characteristics of groundwater around Mt. Meru, Northern Tanzania. Applied Water Science, 9(5), 120. doi: 10.1007/s13201-019-0955-3.

Mapsland, 2021. Large topographical map of Tanzania. Accessed 16-07-2021 from https://www.mapsland.com/africa/tanzania/large-topographical-map-of-tanzania.

Nanyaro, J.T., Aswathanarayana, U., Mungure, J.S., Lahermo, P.W., 1984. A geochemical model for the abnormal fluoride concentrations in waters in parts of northern Tanzania. Journal of African Earth Sciences, 2(2), 129–140. doi: 10.1016/S0731-7247(84)80007-5.

737 Parkhurst, D.L., Appelo, C.A.J., 2013. Description of input and examples for PHREEQC
738 version 3 – A computer program for speciation, batch-reaction, one-dimensional transport,
739 and inverse geochemical calculations: U.S. Geological Survey Techniques and Methods,
740 book 6, chap. A43, 497 p. Accessed 29-09-2019 from http://pubs.usgs.gov/tm/06/a43.
741 Sawyer, G.M., Carn, S.A., Tsanev, V.I., Oppenheimer, C., Burton, M., 2008. Investigation into
742 magma degassing at Nyiragongo volcano, Democratic Republic of the Congo.
743 Geochemistry, Geophysics, Geosystems, 9 (2), American Geophysical Union and
744 Geochemical Society. doi:10.1029/2007GC001829.
745 Scoon, R.N., 2018. Arusha national park (Mount Meru). In: Geology of national parks of
746 central/southern Kenya and Northern Tanzania. Springer, Cham. pp. 141–154. doi:
747 10.1007/978-3-319-73785-0_13.
748 Tanzania Bureau of Standards, 2008. TZS 789:2008: Drinking (potable) water – Specification.
749 Dar es Salaam, Tanzania.
750 Tanzania National Bureau of Statistics, 2013. 2012 population and housing census: Population
751 distribution by administrative areas. Tanzania National Bureau of Statistics, Dar es
752 Salaam. Accessed 26-11-2020 from
753 https://www.nbs.go.tz/nbs/takwimu/census2012/Census_General_Report.zip.
754 Tomašek, I., Mouri, H., Dille, A., Bennett, G., Bhattacharya, P., Brion, N., Elskens, M.,
755 Fontijn, K., Gao, Y., Gevera, P.K., Ijumulana, J., Kisaka, M., Leermakers, M., Shemsanga,
756 C., Walraevens, K., Wragg, J., Kervyn, M., 2022. Naturally occurring potentially toxic
757 elements in groundwater from the volcanic landscape around Mount Meru, Arusha,
758 Tanzania and their potential health hazard. Science of The Total Environment, 807(1),
759 150487. doi: 10.1016/j.scitotenv.2021.150487.
760 Tóth, J., 1963. A theoretical analysis of groundwater flow in small drainage basins. Journal of
761 Geophysical Research, 68 (16), 4795–4812. doi: 10.1029/JZ068i016p04795.
762 Tóth, J., 1999. Groundwater as a geologic agent: An overview of the causes, processes, and
763 manifestations. Hydrogeology Journal, 7, 1–14. doi: 10.1007/s100400050176.
764 Walraevens, K., Bakundukize, C., Mtoni, Y.E., Van Camp, M., 2018. Understanding the
765 hydrogeochemical evolution of groundwater in Precambrian basement aquifers: A case
766 study of Bugesera region in Burundi. Journal of Geochemical Exploration, 188, 24-42.
767 doi: 10.1016/j.gexplo.2018.01.003.
768 Wilkinson, P., Downie, C., Cattermole, P.J., Mitchell, J.G., 1983. Arusha, Geological Survey
769 of Tanzania, Quarter degree sheet 55. Accessed 15-06-2017 from
770 https://library.wur.nl/WebQuery/file/isric/fulltext/isricu_i33425_001.pdf.

771 World Health Organization (WHO), 2017. Guidelines for drinking-water quality: fourth edition
772 incorporating the first addendum. Geneva, World Health Organization. Accessed 12-02-
773 2020 from https://apps.who.int/iris/bitstream/handle/10665/254637/9789241549950-
774 eng.pdf?sequence=1.
775 Wu, J., Li, P., Qian, H., 2015. Hydrochemical characterization of drinking groundwater with
776 special reference to fluoride in an arid area of China and the control of aquifer leakage on
777 its concentrations. Environmental Earth Sciences, 73(12), 8575–8588. doi:
778 10.1007/s12665-015-4018-2.
779